

From Grayscale Photopolymerization 3D Printing to Functionally Graded Materials

Guanghai Fei,* Cesar Parra-Cabrera, Kuo Zhong, Koen Clays, and Rob Ameloot*

Functionally graded materials (FGMs) have spatial variations in structure or composition that result in gradients in their mechanical, thermal, swelling, or other properties. FGMs have garnered significant research interest because of their extensive applications in areas such as biomedical implants, sensors, and soft robotics. Recently, grayscale photopolymerization 3D printing has emerged as a promising technology for crafting complex and high-resolution FGMs. This comprehensive work delves into various grayscale photopolymerization 3D printing techniques, offering insights into their ability to precisely control printing exposure energy and polymerization degree, which in turn influence material properties. Furthermore, this work highlights diverse applications of grayscale vat-photopolymerization 3D printing. Finally, it offers perspectives on ways to enhance grayscale photopolymerization 3D printing, with a focus on improving printing feedstocks and grayscale strategies.

1. Introduction

Unlike homogeneous materials, functionally graded materials (FGMs) exhibit variation in their mechanical, electrical, thermal, or magnetic properties.^[1-4] The inception of FGMs can be traced back to their use as thermal barrier materials in the Japanese space program, where heat-resistant ceramics were placed on the high-temperature side, and tough metals with high thermal conductivity were placed on the low-temperature side, with a gradual change in composition from ceramic to metal

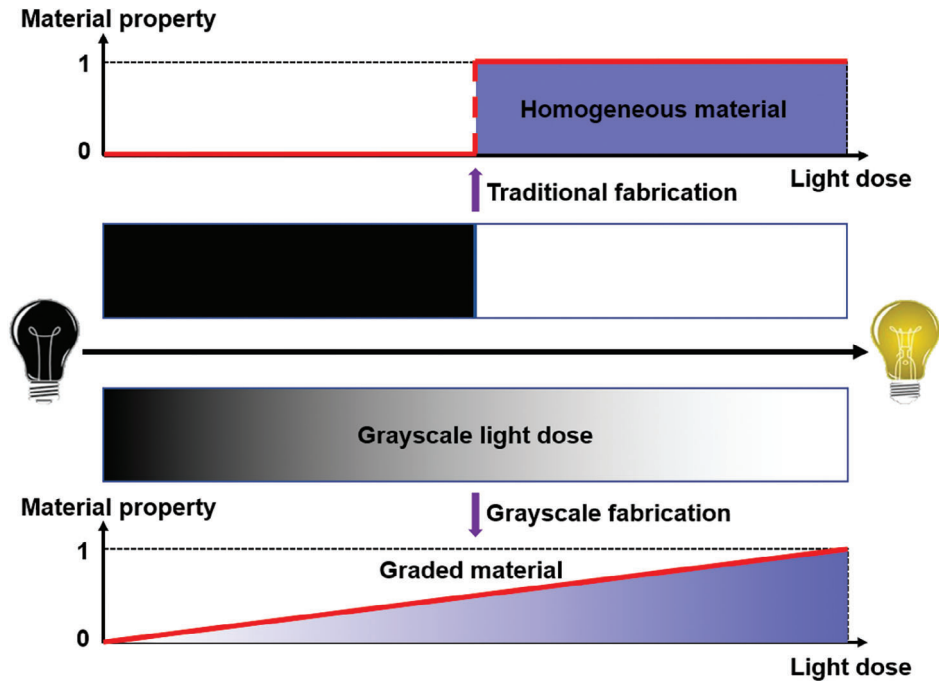
occurring between the two sides.^[5] Since that pioneering application, FGMs have found widespread utility in diverse fields such as actuators/robots,^[6-8] biomedical implants,^[9,10] energy absorption devices,^[11-13] and sensors.^[12] Conventional techniques for fabricating materials with 1D or 2D gradients include gas-phase techniques (e.g., thermal spray, surface reaction), liquid-phase methods (e.g., casting, electrophoretic deposition), and solid-phase approaches (e.g., laser deposition, powder metallurgy).^[1,14] However, these techniques fall short in their ability to customize the properties of FGMs in 3D, and it remains a challenge to develop novel techniques that can create 3D property gradients to meet the demand for complex and multi-functional FGMs in various applications.

The application of 3D printing has opened up new possibilities for fabricating FGMs with 3D property gradients.^[15-22] Among the various 3D printing techniques, vat-photopolymerization (VP) 3D printing stands out as particularly promising for creating complex parts with high resolution and speed.^[23-25] However, traditional VP 3D printing is not suitable for fabricating FGMs because it involves printing a single photoresin feedstock under constant-intensity irradiation throughout the entire printing process, thereby producing homogeneous materials (**Scheme 1**). In contrast, grayscale VP 3D printing techniques enable the precise control of light dosage by modifying the gray value. This results in a material with one or more gradients in properties such as density, hardness, stiffness, or surface roughness (**Scheme 1**).

This Review categorizes the family of grayscale VP 3D printing methods into several branches, each enabling precise control of the exposure dose during polymerization. These branches include laser-based grayscale 3D printing (modifying power or scan speed in grayscale direct laser writing setups), projection-based grayscale 3D printing (tuning the exposure intensity via grayscale masks or varying exposure time via dynamic digital exposure), and volumetric grayscale 3D printing (modifying the exposure intensity, similar to the projection-based method). We commence our discussion with an overview of VP 3D printing, encompassing its fundamental principles, techniques, and mechanisms. Subsequently, we delve into the various grayscale techniques for managing the degree of polymerization and its material properties. Finally, we summarize recent literature on grayscale photopolymerization applications in microfluidics, micro-optics, gradient-color printing, biomedical systems, soft robotics, and

G. Fei, C. Parra-Cabrera, R. Ameloot
Centre for Membrane Separations
Adsorption
Catalysis and Spectroscopy (cMACS)
KU Leuven
Celestijnenlaan 200F, Leuven 3001, Belgium
E-mail: guanghaifei@gmail.com; rob.ameloot@kuleuven.be

G. Fei
Advanced Institute for Life and Health
Zhongda Hospital
Southeast University
Dingjiaqiao 87, Nanjing 210009, China
K. Zhong, K. Clays
Department of Chemistry
KU Leuven
Celestijnenlaan 200D, Leuven 3001, Belgium



Scheme 1. Comparison between traditional and grayscale photopolymerization. In traditional photopolymerization, the light source switches between “ON” and “OFF”, resulting in a single, homogeneous material (where the photoresin polymerizes only when the light is “ON”). In contrast, grayscale photopolymerization varies the exposure dose using different gray levels. When triggering polymerization of the photoresin, these different exposure doses result in varying degrees of resin monomer conversion (i.e., cross-linking), thereby creating materials having gradients in their mechanical, thermal, or swelling properties.

origami (Figure 1). The great success of grayscale VP 3D printing in the production of FGMs indicates its promise as a fabrication tool for broadening the utility of photopolymerization 3D printing.^[26–32]

2. Vat-Photopolymerization 3D printing

In the years since Hull coined the term “stereolithography” (SLA) in 1986,^[33] VP 3D printing has come to encompass various photopolymerization printing processes employing a range of light sources, motion control, and polymerization mechanisms. All these photopolymerization printing processes use a light source to selectively trigger polymerization in photosensitive materials. Here, we briefly discuss the progress and evolution of recent VP 3D printing techniques, which have evolved from serial to planar and volumetric build platforms. In addition, we provide an overview of the commonly employed photopolymerization mechanisms.

2.1. Vat-Photopolymerization 3D Printing Techniques

There are two main serial VP 3D printing technologies: laser scan SLA and two-photon polymerization (TPP). Laser scan SLA constructs objects by the raster-like scanning of a laser beam beneath the surface of a photoresin (upper panel in Figure 2A). Typically, a pair of mirrors within a Galvano scanner controls the position of the beam. The slice information is represented as a set of coordinates (scan lines) that determine the tilt angle of the two mirrors,

guiding the laser beam’s path along the plane. TPP uses a high-power femtosecond-pulsed near-infrared (NIR) laser to solidify regions within a vat of photopolymerizable resin (lower panel in Figure 2A). Only the photoresin at the laser’s focal point undergoes polymerization, as the surrounding areas are effectively transparent to the long-wavelength light and do not receive sufficient energy to initiate polymerization. By tracing the laser’s focal point in 3D space, TPP allows for the free-form fabrication of intricate 3D structures.

The development of projection 3D printing represented a paradigm shift from serial printing to planar printing. Instead of using a raster-scanned laser, projection 3D printing employs a dynamically changing “digital mask” through a spatial light modulator to project 2D patterns (object slices) onto the resin bed. Concurrently, the build platform adjusts its height for each layer. Unlike conventional laser scan SLA, which operates linearly, projection-based VP fabricates the entire object plane simultaneously, substantially reducing build time. In projection 3D printing, the light modulator is integral to the printing process. Three types of light modulator elements have been used to generate digital masks: liquid crystal displays (LCDs),^[34–36] digital micromirror devices (DMDs),^[37,38] and liquid crystals on silicon (LCoS).^[7,39,40] An LCD contains layers of liquid crystals and electrodes sandwiched between polarizing filters; incoming light is modulated by applying an electrical current to the electrodes in specific areas, causing the liquid crystals to align and block the passage of light.^[36,41] A DMD comprises arrays of micromirrors on individually addressable tilt switches, where each micromirror has an “ON” or “OFF” state that allows selective reflection of incoming light. The desired 2D patterns are created by

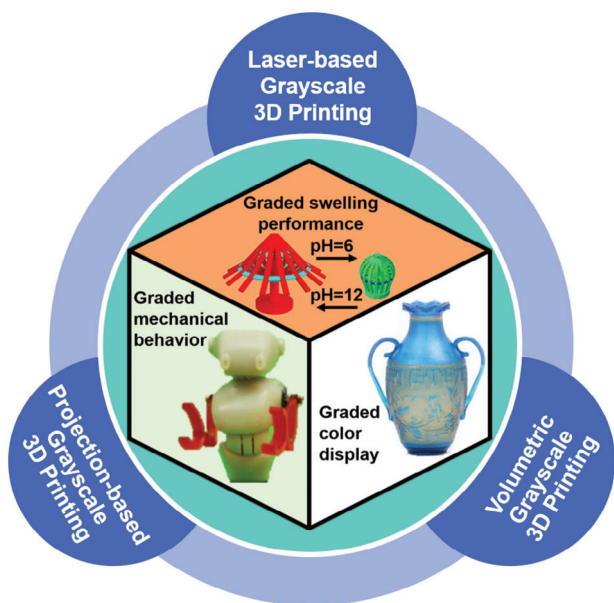


Figure 1. An overview of grayscale photopolymerization 3D printing techniques for graded materials, with a focus on both methods (outer layer) and applications (center). Top panel adapted with permission.^[8] Copyright 2020, Elsevier. Left side panel adapted with permission.^[26] Copyright 2019, American Association for the Advancement of Science. Right side panel adapted with permission.^[28] Copyright 2022, Wiley-VCH.

toggle individual mirrors in selected areas.^[41,42] An LCoS modulator similarly patterns the light field by energizing selected pixels on a reflective liquid crystal chip.^[39]

There are two main projection-based VP 3D printing technologies: layer-by-layer projection (upper panel in Figure 2B) and continuous projection printing (lower panel in Figure 2B). The difference lies in whether the cured parts are separated from the fabrication interface after each exposure: layer-by-layer projection requires separation, whereas continuous projection does not. Two recent techniques for continuous projection 3D printing are continuous liquid interface production (CLIP)^[23] and high-area rapid printing (HARP).^[43] In these continuous projection printing techniques, an oxygen-permeable membrane (in CLIP) or a mobile liquid interface containing fluorinated oil (in HARP) is strategically placed at the fabrication window to inhibit polymerization and minimize adhesion between the printed part and the fabrication interface, which is a critical factor in enabling continuous projection SLA. These techniques significantly accelerate the printing process, e.g., a 38 cm × 61 cm × 76 cm object was completed via HARP in just 1 h 45 min,^[43] whereas the layer-by-layer method would take 10–20 h to create the same object.

Volumetric 3D printing has been developed to significantly enhance printing speed, which solidifies centimeter-sized objects within tens of seconds.^[25,44] This cutting-edge technology constructs an object in a single step by irradiating a transparent resin bath from multiple directions.^[25,44–46] Two notable examples of volumetric 3D printing techniques are computed axial lithography (CAL)^[44] and xolography.^[25] CAL uses a digital projector to project intensity-modulated images in synchronization with the rotational movement of the resin container (upper panel in Figure 2C). The superposition of exposures from

multiple angles generates a 3D energy dose sufficient to solidify the material into the desired geometry.^[44,47,48] Xolography uses photoswitchable photoinitiators to induce local polymerization within a monomer volume upon linear excitation arising from intersecting light beams of different wavelengths (lower panel in Figure 2C).^[25] Xolography reportedly has a resolution approximately ten times better than that of CAL and a volume generation rate that is four to five orders of magnitude higher than that of TPP.^[25]

Table 1 provides a summary of the advantages and disadvantages associated with each VP 3D printing technique. TPP has the best resolution (≈ 100 nm) and laser scan SLA has the worst (≈ 50 μ m). CAL and xolography emerge as the top choices for speed, followed by CLIP and HARP, with TPP being the slowest. Layer-by-layer projection VP has only moderate speed and resolution, but it exhibits the greatest potential for integration with emerging printing strategies, such as grayscale or multi-material methods.

2.2. Photopolymerization Mechanisms

This section offers a concise overview of the underlying mechanisms, monomers, and photoinitiators used in VP polymerization reactions. We refer the reader to Review articles on special topics of radical^[61] and cationic^[62] polymerization for more comprehensive overviews.

Radical polymerization is the most commonly used method in VP 3D printing processes. It is characterized by a sequence of reactions: initiation, propagation, and termination.^[61] The process can be summarized as follows: i) light strikes a photoinitiator, generating free-radical species; ii) these free radicals interact with functional monomers to form active monomers; iii) active monomers then engage in radical propagative reactions with other monomers, leading to the production of polymeric chains until termination of the reaction.^[41,61] (Meth)Acrylate monomers and thiol-ene/thiol-yne systems constitute two common categories of radical-polymerizable mediums employed in VP 3D printing (Table 2). Radical photoinitiators can be categorized into two groups based on their mechanism of radical generation: type I, which uses cleavable photoinitiators, and type II, which employs bimolecular photoinitiating systems. Most commercially available photoinitiators undergo type I cleavage, resulting in the generation of radical fragments upon irradiation. This category includes compounds such as 2-hydroxy-2-methylpropiophenone (Irgacure 1173), 1-hydroxycyclohexylphenylketone (Irgacure 184), diphenyl(2,4,6-trimethyl benzoyl)phosphine oxide (TPO), and lithium phenyl-2,4,6-trimethylbenzoyl phosphinate (LAP) (Table 2). Type II systems consist of an uncleavable sensitizer and a co-initiator, typically forming excited triplet states under light exposure. Commonly used uncleavable photoinitiators, such as camphorquinone (CQ), benzophenone, 2',4',5',7'-tetrabromofluorescein disodium salt (EY), and thioxanthone, have the capacity to undergo hydrogen-abstraction or electron-transfer reactions in the presence of co-initiators.^[63]

Cationic polymerization is another crucial process in VP 3D printing. It was initially developed in the 1970s to address the limitations of radical polymerization, such as its high sensitivity to oxygen.^[62] The typical mechanism of cationic photoinitiation

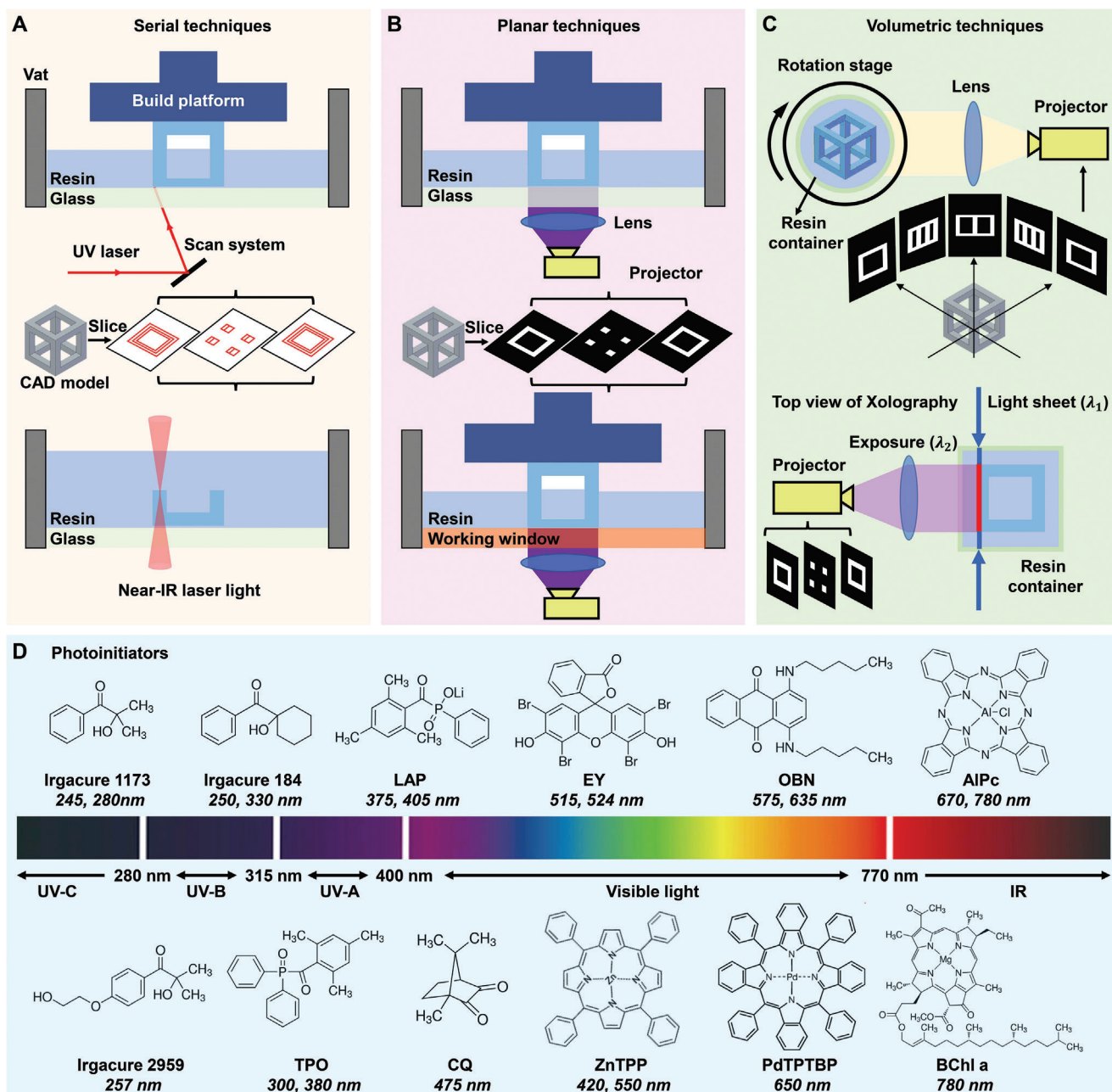


Figure 2. Vat-photopolymerization 3D printing techniques and examples of photoinitiators/photocatalysts used for photopolymerization. A) Serial techniques: laser scan stereolithography (SLA) and two-photon polymerization (TPP). The computer-aided design (CAD) model is sliced into a series of 2D scan-line images. Based on the slice information, a laser selectively solidifies the photopolymerizable resin at the vat surface (upper panel, laser scan SLA with a continuous beam) or within the vat (lower panel, TPP with a femtosecond pulse near-infrared laser). B) Planar techniques: projection-based 3D printing (layer-by-layer or continuous). The CAD model is sliced into a stack of 2D black-and-white images, which are projected one by one onto the resin bed while the build platform changes height for each image. Fabrication can be carried out layer-by-layer (upper panel) or continuously (lower panel). C) Volumetric techniques: computed axial lithography (CAL) and xolography. Volumetric construction can be achieved by projecting digital patterns (inspired by X-ray computed tomography reconstruction projections) into a rotating vat (upper panel, CAL) or by using photoswitchable photoinitiators to induce local polymerization within a confined monomer volume through linear excitation caused by intersecting light beams of different wavelengths (lower panel, xolography). D) Examples of photoinitiators/photocatalysts used in photopolymerization (with absorption peaks from ultraviolet to infrared light as indicated by the bottom numbers). Irgacure 1173: 2-hydroxy-2-methylpropiophenone; Irgacure 2959: 2-hydroxy-4'-(2-hydroxyethoxy)-2-methylpropiophenone; Irgacure 184: 1-hydroxycyclohexylphenylketone; TPO: diphenyl(2,4,6-trimethyl benzoyl)phosphine oxide; LAP: lithium phenyl-2,4,6-trimethylbenzoyl phosphinate; CQ: camphorquinone; EY: 2',4',5',7'-tetrabromofluorescein disodium salt; ZnTPP: zinc tetraphenylporphyrin; OBN: oil blue N; PdTPBP: photoinitiators like palladium(II) meso-tetraphenyltetrabenzoporphyrin; AIPc: aluminum phthalocyanine; BChl a: bacteriochlorophyll a. Reproduced with permission.^[49] Copyright 2019, American Chemical Society.

Table 1. Comparison of vat-photopolymerization 3D printing techniques^{a)}.

Type	Description	Advantages	Drawbacks
Laser scan SLA	Laser triggers polymerization within a vat in a raster-like contactless manner	Using high-power laser is advantageous for printing filler-loaded suspensions	* 20 mm/h (z axis) ^[50] * Poor resolution ($\approx 50 \mu\text{m}$) ^[51,52] * Support needed
TPP	A femtosecond-pulsed near-infrared laser is used to solidify regions within a photopolymerizable vat in a serial and contactless manner	Nanometer resolution ($\approx 100 \text{ nm}$) ^[51,53]	* $1\text{--}20 \text{ mm}^3 \text{ h}^{-1}$ (whole printing) ^[54,55] * Small build volume ($<1 \text{ cm}^3$) ^[51,56,57] * Requirements for materials (highly transparent and well-dispersed)
Layer-by-layer projection	Projection of digital slices into a stationary vat layer-by-layer; includes LCD-based and DMD-based techniques	<ul style="list-style-type: none"> ✓ Overhanging structures ✓ Scalable build volume ($1\text{--}125 \text{ cm}^3$)^[51] ✓ Micrometer resolution ($\approx 10 \mu\text{m}$)^[51,58] ✓ Potential to integrate with emerging technologies 	Staircase effect
Continuous projection	Continuous production is achieved by positioning an oxygen-permeable membrane (in the case of CLIP) or a mobile liquid interface containing fluorinated oil (in the case of HARP) at the fabrication window	<ul style="list-style-type: none"> ✓ 3000 mm h^{-1} (z axis)^[23,59] ✓ Overhanging structures ✓ Scalable build volume ✓ Micrometer resolution 	Difficult to incorporate with multi-material printing
CAL	Volumetric build by projecting digital patterns into a rotating vat	<ul style="list-style-type: none"> ✓ $30\text{--}120 \text{ s}$ (centimeter-scale object)^[45,60] ✓ One-step fabrication ✓ Support-free 	Requirements for materials (highly transparent and well-dispersed)
Xolography	Uses photoswitchable photoinitiators to induce local polymerization inside a confined monomer volume upon linear excitation by intersecting light beams of different wavelengths	<ul style="list-style-type: none"> ✓ $\approx 60 \text{ s}$ (centimeter-sized object), $\approx 55 \text{ mm}^3 \text{ s}^{-1}$^[25] ✓ One-step fabrication ✓ Micrometer resolution ✓ Support-free 	Requirements for materials (highly transparent and well-dispersed)

^{a)} Abbreviations: SLA: stereolithography; TPP: two-photon polymerization; CAL: computed axial lithography; LCD: liquid crystal display; DMD: digital micromirror device; CLIP: continuous liquid interface production; HARP: high-area rapid printing

unfolds as follows: when exposed to irradiation, cationic photoinitiators undergo homo- or heterolytic cleavage, resulting in a mixture of cations, radical cations, and radical intermediates. Although these reactive intermediates can initiate radical or cationic polymerization directly, they often further react with hydrogen donors (e.g., the solvent or a monomer) to generate Brønsted acids, which, in turn, initiate the polymerization.^[62,64] For photoinduced cationic cross-linking reactions, onium salts (e.g., bis(4-*tert*-butylphenyl)iodonium hexafluorophosphate, Ph_2IPF_6 , triarylsulfonium hexafluoroantimonate salts) are frequently employed (Table 2) because they can initiate most cationic polymerizations, including those of epoxides, oxetanes, and vinyl ethers.^[65]

Hybrid systems that combine both radical and cationic polymerizations are quite prevalent in the production of photoresins. One example involves the synthesis of epoxide-acrylate hybrid oligomers, which are used to reduce the oxygen inhibition of the radical process and enhance toughness and adhesion properties.^[66–69] In addition, a novel continuous multi-material technique, wavelength-selective photopolymerization, has been developed recently to initiate radical and cationic polymerizations in specific locations using light sources of two different wavelengths.^[70–76]

The selection of the photoinitiator depends on the nature of the light source (Figure 2D). For printers equipped with a deep-UV light source (e.g., laser scan SLA, $\approx 330 \text{ nm}$), photoinitiators like Irgacure 1173,^[77–80] Irgacure 2959 (2-hydroxy-

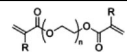
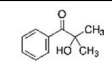
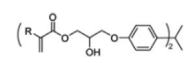
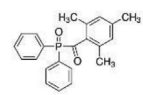
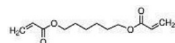
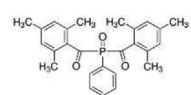
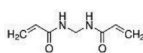
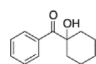
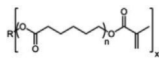
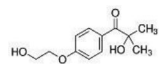
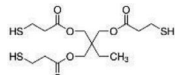
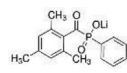
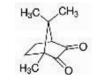
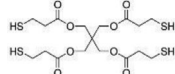
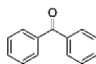
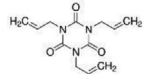
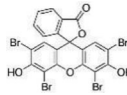
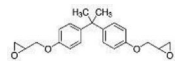
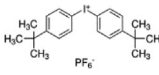
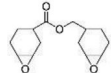
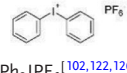
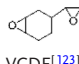
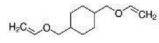
4'-(2-hydroxyethoxy)-2-methylpropiophenone),^[72,81–86] and Irgacure 184^[80,87–89] are suitable choices. In projection photopolymerization machines using UV or blue light, TPO,^[80,90–93] LAP,^[85,86,94,95] and CQ^[63,70,72,76,93] are commonly used (TPO and LAP for UV light, 370–405 nm; CQ for blue light, $\approx 475 \text{ nm}$). For visible-light-induced VP 3D printing (450–635 nm), EY,^[85,96–99] zinc tetraphenylporphyrin,^[100,101] and oil blue N^[102] are the preferred photoinitiators. For TPP machines with red or IR light sources ($\approx 780 \text{ nm}$), photoinitiators like palladium(II) *meso*-tetraphenyltetraabenzoporphyrin,^[24] aluminum phthalocyanine,^[103] and bacteriochlorophyll a^[104] are commonly employed.

3. Grayscale Photopolymerization Technologies

3.1. Serial Technique: Laser-Based Grayscale 3D Printing

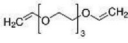
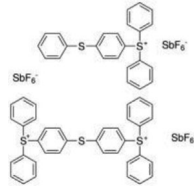
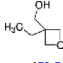
In laser-based VP 3D printing (including laser scan SLA and TPP), each voxel of the object is irradiated sequentially. This process theoretically enables the adjustment of the exposure dose by varying the laser writing parameters, such as the laser power, laser scanning speed, or the distance between two scanning lines/layers (Equation 1 in Table 3). As a result, there is precise control over the local cross-linking degree within the resin matrix (Figure 3A–C), leading to the development of graded properties (e.g., stiffness and swelling/shrinking degree). Alter-

Table 2. Photopolymerization mechanisms^{a)}.

Type	Monomer	Photoinitiator	Absorption	
Radical	(Meth)Acrylate monomers			200–300 nm
		PEG-D(M)A ^[27,81,94,105–110] (R=H or CH ₃)	Irgacure 1173 ^[77–80]	
				220–400 nm
		DGEBA-D(M)A ^[101,111–113] (R=H or CH ₃)	TPO ^[80,90–93]	
				220–400 nm
		HDDA ^[111,114,115]	Irgacure 819 ^[27,80,105–107,109,116]	
				220–400 nm
		MBAA ^[82,83,95]	Irgacure 184 ^[80,87–89]	
				257–365 nm
		PCL-MA ^[117–120]	Irgacure 2959 ^[72,81–86]	
Thiol-ene and thiol-yne systems			325–425 nm	
		Trithiol ^[102]	LAP ^[85,86,94,95]	
			400–500 nm	
		CQ ^[63,70,72,76,93]		
				250–350 nm
		PETMP ^[72,121]	Benzophenone ^[63,91]	
		425–525 nm		
TTT ^[72,122]	Eosin Y ^[85,96–99]			
Cationic	Epoxides			325–425 nm
		DGEBA ^[123,124]	Iod ^[101,125]	
				300–455 nm
		EPOX ^[76,101,102]	Ph ₂ IPF ₆ ^[102,122,126]	
	Oxetanes and vinyl ethers		350–500 nm	
				
		CDVE ^[124,127]		

(Continued)

Table 2. (Continued)

Type	Monomer	Photoinitiator	Absorption
	 DVE-3 ^[79,102,127]	 TAS ^[70,71,127,128]	350–400 nm
Hybrid	Composite	Acrylate, Epoxy	CQ ^[70] (or I-819) ^[71] + TAS
	 OXA ^[73,76]		wavelength-selective polymerization 365 and 450 nm

^{a)} Abbreviations of materials: PEG-DA, poly(ethylene glycol) diacrylate; PEG-MA, poly(ethylene glycol) dimethacrylate; Irgacure 1173, 2-hydroxy-2-methylpropiophenone; DGEBA-DA, bisphenol A diglycidyl ether diacrylate; DGEBA-MA, bisphenol A-glycidyl methacrylate; TPO, diphenyl(2,4,6-trimethylbenzoyl) phosphine oxide; HDDA, 1,6-hexanediol diacrylate; Irgacure 819, phenylbis(2,4,6-trimethylbenzoyl) phosphine oxide; MBAA, *N,N'*-methylenebis(acrylamide); Irgacure 184, 1-hydroxycyclohexyl phenyl ketone; PCL-MA, poly(*ε*-caprolactone) methacrylate; Irgacure 2959, 2-hydroxy-4'-(2-hydroxyethoxy)-2-methylpropiophenone; NIPAAm, *N*-isopropylacrylamide; LAP, lithium phenyl-2,4,6-trimethylbenzoyl phosphinate; Trithiol, trimethylolpropane tris(3-mercaptopropionate); CQ, camphorquinone; PETMP, pentaerythritol tetra(3-mercaptopropionate); TTT, triallyl-1,3,5-triazine-2,4,6-(1*H*,3*H*,5*H*)-trione; Eosin Y, 2',4',5',7'-tetrabromofluorescein disodium salt; DGEBA, bisphenol A diglycidyl ether; Iod, bis(4-*tert*-butylphenyl)iodonium hexafluorophosphate; EPOX, (3,4-epoxycyclohexyl)methyl 3,4-epoxycyclohexanecarboxylate; Ph₂IPF₆, diphenyliodonium hexafluorophosphate; VCDE, vinylcyclohexene dioxide; CDVE, 1,4-cyclohexanedimethanol divinyl ether; 2,4,6-TAP fluoroborate, 2,4,6-tris(4-methoxyphenyl) pyrylium tetrafluoroborate; DVE-3, tri(ethylene glycol) divinyl ether; TAS, triarylsulfonium hexafluoroantimonate salts; OXA, (3-ethyloxetan-3-yl)methanol.

ing the laser power is a prevalent technique for controlling exposure dosage; in general, an increase in exposure dosage facilitated the cross-linking of more polymer chains to form a denser polymer network (Figure 3A).^[8,129] Adjusting the laser scanning speed is another common strategy for controlling the exposure dosages of the laser and the graded properties of the print (Figure 3B). The local cross-linking degree within the resin matrix decreases with the increase in printing speed because a high scan speed results in a short residence time (and consequently, a low exposure dosage).^[130] In addition to adjusting laser power and laser scanning speed, researchers have changed the “layer thickness” (the distance between two scanning layers) in TPP or the “hatch spacing” (the distance between two scanning lines) in laser scan SLA to modify the local cross-linking degree of the resin matrix.^[131,132] In TPP, all points lying in the same plane are fabricated together, with the laser focus then moving to the next layer to fabricate the set of points lying on that plane; a higher distance between two adjacent scanning layers forms looser polymer networks (Figure 3C). In laser scan SLA, objects are constructed through the raster-like scanning of a laser beam; a higher hatch spacing forms looser polymer networks between two scanning lines.

3.2. Planar Technique: Projection-Based Grayscale 3D Printing

Although various VP technologies are available, projection-based VP has emerged as the most widely adopted method for grayscale 3D printing. Because the polymerization degree of the photoresin is controlled by the exposure dose (mJ cm^{-2}), and the latter is the product of the intensity of the light source (mW

cm^{-2}) and the exposure time (s), grayscale 3D printing can be achieved either by spatial control over the light intensity or by the exposure time (Equation 2 in Table 3). The resulting gradient in the cross-linking degree within the resin matrix leads to corresponding gradients in properties such as mechanical, thermal, or swelling.

Digital grayscale masks are a prevalent technique in grayscale 3D printing for controlling light intensity (Figure 3D–F). These digital grayscale patterns are loaded into the printers and projected using DMD/LCoS modulators (reflectance projection printers) or displayed through an LCD (transmission projection printer). Among the digital grayscale masks, the most commonly employed are the 8-bit and halftoning patterns (Figure 3D,E). For 8-bit patterns, grays are encoded in bit planes that represent the ratio of light states to dark. Each pixel's relative brightness is defined in the bitwise segment, with each bit indicating successive ON/OFF durations.^[133] In this technology (using DMD as an example, Figure 3D), grayscale does not represent true gray colors; instead, the DMD projector switches mirrors ON and OFF at a 1/256 duty cycle.^[42,133] As indicated in Table 3, high-end printers or custom systems can directly project the grayscale mask pattern. However, many commonly used projection SLA printers can only handle 1-bit slices.^[35,36,87,88,134,135] In such cases, 1-bit binary grayscale masks (comprising binary black and white pixels) generated through halftoning algorithms offer simpler and more universally applicable alternatives.^[136–139] Two commonly used pixel-coding algorithms, namely the frequency-modulated and amplitude-modulated methods,^[136,140,141] have been employed to create binary masks with different brightness levels by arranging black and white pixels in varying ratios.

Table 3. Comparison of various grayscale 3D printing techniques.

Technology	Type	Advantages	Drawbacks	Representative printers
Serial: laser-based method ^{a)}	Laser scan stereolithography (SLA)	High power enables grayscale 3D printing with composite formulations	Most commercial laser SLA printers can not modify the parameters layer-by-layer	✓ Moai Laser SLA 3D Printer (Peopoly, laser-based), ^[156] \$3099
	Two-photon polymerization (TPP)	Very high resolution: spatial control over the cross-linking degree at a nanometer scale	* 1–20 mm ³ h ⁻¹ (whole printing) ^[54,55] * Small build volume (≈ 1 cm ³) ^[51,56] * Limited material selection	✓ Photonic Professional GT (Nanoscribe GmbH, direct laser writing), ^[53,157] \$350 000
Planar: projection-based method ^{b)}	8-bit grayscale masks	✓ Mainstream approach ✓ Pixel-level resolution ✓ Rapid: different gray level exposures synchronously	High-end printers or custom systems are needed	✓ NanoArch S130/S140 (BMF, DMD-based), ^[158] \$50 000 to \$120 000 ✓ Ember 3D Printer (Autodesk, DMD-based), ^[29] \$5995 to \$7500
	1-bit halftoning masks	✓ Compatible with different commercial SLA printers ✓ Pixel-level resolution ✓ Rapid: different gray level exposures synchronously	* Pixel-coding and image optimization algorithms are needed * Trade-off between print resolution and halftoning printing efficiency ^[141]	Any projection printers
	Digital exposure	✓ Easy to conduct: directly modify the G-codes ✓ Cheap machines	* Different gray level exposures, one by one * Sharp transitions between different gray levels	✓ iSUN3D/Nova3D (LCD-based), ^[112] \$500 to \$1500
	Other technologies	✓ Easy to conduct: physical mask or frontal photopolymerization	Inadequate for preparing complex 3D geometries	Any projection setups
Volumetric method	Xolography and computed axial lithography (CAL)	No FGMs have been manufactured by volumetric photopolymerization		

^{a)} For serial methods (laser SLA and TPP), the energy delivered can be written as $E = \frac{P}{V_s \times h}$, where E , P , V_s are the energy dose, laser power, and scanning speed, respectively, and h represents the “layer thickness” (the distance between two scanning layers) in TPP^[131] or the “hatch spacing” (the distance between two scanning lines) in laser scan SLA.^[132] Laser-based VP achieves grayscale 3D printing by programming the laser power, scanning speed, or hatch spacing (layer distance) to create a gradient exposure dose. ^{b)} For planar methods (projection-based), the energy delivered can be written as $E = I \times t$, where E , I , t are the exposure dose, light intensity, and exposure time, respectively.^[88,132] Projection VP achieves grayscale 3D printing by programming either light intensity through grayscale masks or exposure time through digital exposure to create a gradient exposure dose.

The so-called “dynamic digital exposure” process^[142–144] represents a special grayscale technique employed in projection SLA (Figure 3F) that closely resembles the grayscale mask method. Whereas the latter achieves this through programming light intensity using grayscale masks, in the former technique, polymerization is controlled by programming the exposure time. Both approaches yield a grayscale exposure dose, resulting in a graded degree of cross-linking. For example, LCD-based and DMD-based projection setups capable of digitally programming exposure times have been used to fabricate functional materials featuring 3D gradients or 4D responsive characteristics.^[112,142] As depicted in Figure 3D–F, a graded lattice sample can be manufactured using an 8-bit grayscale pattern (with gray values of 127, 191, and 255), a 1-bit halftoning pattern (with brightness values of 50, 75, and 100%), or a dynamic digital exposure pattern (with exposure times of 5, 10, and 15 s). Note that the numbers here are indicative only.

3.3. Other Grayscale VP 3D Printing Technologies

In addition to the previously mentioned technologies, various other techniques, including physical or sliding masks and

FPP,^[27,145–150] have been employed to implement grayscale polymerization (Figure 3G–I). Diverse physical grayscale masks have found use in grayscale lithography for creating complex bump topography featuring height and cross-linking degree gradients. This capability enables the production of textured surfaces with micro- and nano-features.^[151–153] For example, an elastic gradient of mercapto-terminated polyvinylmethylsiloxane elastomer was produced using a single physical mask with radial gradual transmittance.^[151] In another example, two overlaid physical masks^[152] were used in the manufacture of a swellable polymer sheet with “smooth” swelling profiles. Other physical masks, such as microfluidic-assisted photomasks, have been used to generate multilevel microstructures.^[153] Apart from physical masks, a sliding mask has been employed to produce a resin sample with varying stiffness, as it creates a linear exposure gradient across the resin when the mask moves. In comparison, FPP achieves a through-thickness gradient in cross-linking degree by light attenuation from the illumination surface into the liquid resin (Figure 3I).^[88,106,112] Based on the modified Lambert-Beer law,^[88] this light attenuation is influenced by both absorption (by photoinitiators) and scattering (from the presence of fillers). It is worth noting that the FPP method is primarily used for

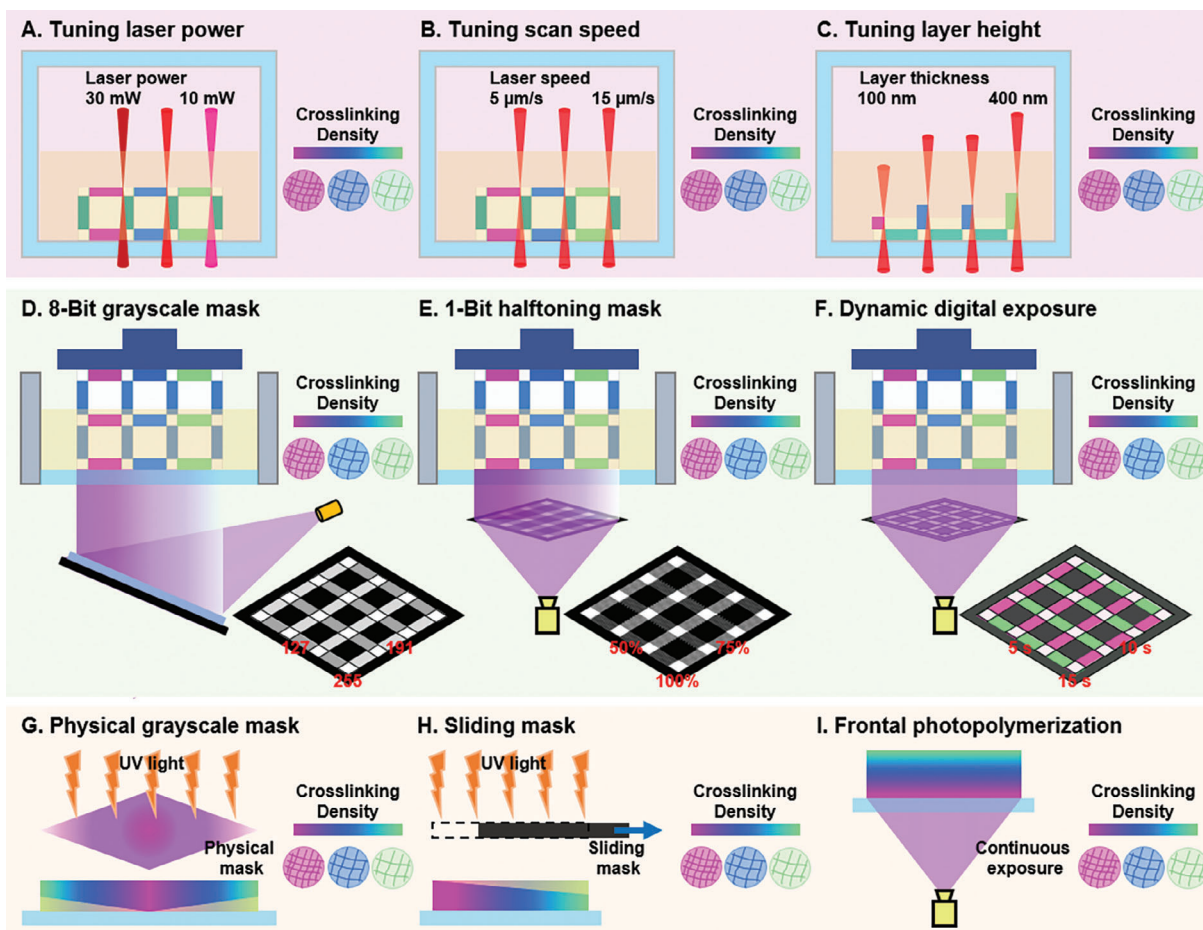


Figure 3. Examples of grayscale vat-photopolymerization 3D printing. A–C) Laser-based grayscale 3D printing technologies (examples based on two-photon polymerization). Grayscale direct laser writing can be achieved through three methods: A) adjusting the laser power, B) fine-tuning the scanning speed, and C) controlling the layer thickness (the distance between each successive layer) during the laser writing process. All these technologies enable voxel control over the local cross-linking degree of the resin matrix. D–F) Projection-based grayscale technologies. Grayscale 3D printing can be accomplished through spatial control over either light intensity (D,E) or exposure time (F). In (D), 8-bit grayscale masks with 256 levels, created in software such as Photoshop or MATLAB, can be used to modulate light intensities during projection, provided that the 3D printer’s light modulator (such as a digital micromirror device or liquid crystals on silicon) can handle grayscale images. Example E) uses 1-bit halftoning masks with opaque/transparent dots generated through pixel-coding algorithms. The fraction of transparent dots defines the brightness level, making it compatible with any projection stereolithography printer. F) Grayscale 3D printing is achieved by assigning different exposure times per voxel, exemplified with a liquid crystal display. In all cases (A–F), the numbers associated with laser parameters and exposure presets are for reference purposes only. G–I) Other grayscale technologies include the use of physical/sliding masks and frontal photopolymerization (FPP) technology. Example G) involves the use of a physical mask with radial gradual transmittance to achieve grayscale printing. Example H) incorporates a sliding mask to create a linear exposure gradient across the resin, resulting in a gradient in cross-linking degree from left (high) to right (low). Example I) describes the grayscale photopolymerization mechanism of FPP: owing to a light intensity gradient in the through-thickness direction, graded cross-linking, and anisotropic volume shrinkage occur when comparing the top of the sample with the bottom.

controlling layer height or cross-linking degree in a single-layer exposure and does not constitute traditional 3D printing. Although these approaches may not be suitable for creating complex 3D geometries (e.g., overhanging features), they present innovative possibilities for expanding the capabilities of VP 3D printing.

3.4. Comparison of Different Grayscale VP 3D Printing Technologies

Table 3 provides a summary of various grayscale VP 3D printing technologies. Among the different grayscale methods employed

in VP 3D printing, grayscale TPP stands out as the preferred choice when high-resolution gradients are required. Projection-based grayscale 3D printing, however, is the dominant approach because of its ability to strike an excellent balance between printing speed and precision.

Of the projection-based grayscale 3D printing techniques (8-bit masks, 1-bit masks, and dynamic digital exposure), the 8-bit grayscale strategy is particularly advantageous because this method employs hexadecimal values to define up to 256 gray levels for each pixel on the mask,^[26–28] resulting in a nearly continuous variation in light intensity during printing.^[152] Conversely, the 1-bit grayscale strategy is compatible with all commercial

projection SLA 3D printers because the digital halftoning method can generate universally printable files consisting only of black and white pixels arranged to mimic the “true” grayscale levels.^[141] In addition to digital grayscale masks, some custom setups and modified commercial printers offer spatial control over exposure time to achieve FGMs.^[105,142–144,154] As a valuable complement to grayscale mask-assisted 3D printing methods, the digital exposure process provides flexible control over exposure energies, enabling a broader range of material properties to be achieved.^[141]

It is worth noting that volumetric 3D printing technologies (xolography and CAL) have not yet been successfully used to create FGMs. The limitations of xolography primarily relate to formulation and scalability. Xolography requires a photoswitchable molecule in the formulation, but there are a limited number of photoswitchable molecules that can be used in 3D printing. Scalability is limited because of light attenuation. A light sheet at a specific wavelength (e.g., 375 nm) excites the molecule from its initial dormant state to a latent state with a finite lifetime. During this excitation, absorption, and scattering along the propagation direction cause attenuation of the light sheet, which ultimately restricts the final print size.^[25] In the case of CAL, the primary challenge lies in controlling exposure dose distribution and mitigating scattering caused by prematurely gelled polymers. During CAL 3D printing, the optical dose delivery is not instant but occurs gradually over time through a projection system. This gradual buildup of local optical dose can result in poor reconstructions, leading to undesired extra gelation or premature gelation in high-dose voxels. Moreover, these prematurely gelled regions can scatter subsequent writing beams, disrupting the completion of dose delivery to the rest of the printed part.^[155]

4. Applications of Grayscale Photopolymerization

4.1. Microfluidics and Micro-Optics

According to the Lambert-Beer law and SLA working curves,^[88,159] varying cure depths can be achieved by exposing a photoresin to grayscale light doses during single-layer fabrication. This technique facilitates the production of microstructures with intricate or modulated topographies, making them well-suited for use in microfluidic and micro-optic components, although it is worth noting that care must be taken when using these techniques to avoid overexposure of adjacent regions and thereby polymerizing void features.^[105,160] He et al. employed grayscale dual-projection lithography to create circular microfluidic channels.^[161] They used two projectors to project grayscale images toward each other, enabling simultaneous material polymerization. During this process, a circular region was formed in areas with low light intensity; the overlap of energy at the interface of the upper-half and lower-half parts facilitated bonding between them (**Figure 4A**). This approach created customized circular microchannels with intricate features such as junctions, bifurcations, hierarchies, and gradually changing diameters. Rammohan et al. fabricated multilevel microstructures in a single step by manipulating structure shape, dimensions, and grayscale values in the grayscale mask.^[162] **Figure 4B** illustrates a 150 μm wide microchannel (left) and an embedded microchannel with alternating obstructions (middle) created for a passive mixer (right). Atencia et al. fabricated

microfluidic structures with 3D topographies by using binary grayscale (halftoning) masks.^[138] A single-step grayscale exposure generated a multilevel microchannel network with varying widths and heights (**Figure 4C**, left) and curved surfaces (right). Nordin et al. achieved significantly higher-resolution 3D components beyond the limitations of an SLA printer by assigning different exposure times per pixel (**Figure 4D**). These multilevel microstructures and modulated topographies have the potential to facilitate various applications that leverage the microscale manipulation of liquids. For example, they can enhance chaotic advection to promote mixing^[162,163] and enable the integration of valves and pumps into microfluidic systems.^[138,164]

Grayscale VP also offers the capability to produce optical microcomponents. For example, two distinct methods—grayscale electron beam lithography and grayscale stencil-assisted electron beam deposition—were employed to craft layered structures with spatial thickness variations for multispectral filter arrays (**Figure 5A**). Valentine et al. applied grayscale nanosphere lithography to fabricate optic metasurfaces with arbitrary, nonperiodic phase profiles (**Figure 5B**). Yuan et al. achieved the simultaneous fabrication of microlenses of various sizes and profiles with excellent shape fidelity, low surface roughness (≈ 5 nm), and high imaging resolution (line width: 1.639 μm) by combining single grayscale UV exposure with mechanical oscillation.^[165] **Figure 5C** presents the designed grayscale pattern alongside the printed hybrid concave-convex microlens array: a triangular array comprising six concave microlenses surrounded by 15 convex ones. Similarly, a “drosophila eye” compound microlens array has been replicated using a bio-inspired grayscale mask (**Figure 5D**). This textured surface, created through grayscale lithography, can modify its hydrophobicity, friction, haptics, and adhesion.^[166,167]

4.2. Biomedical Applications

Grayscale VP 3D printing holds significant promise for biomedical applications (such as tissue engineering, organs-on-chips, and drug screening) because of its ability to fabricate sophisticated miniature biological constructs with graded properties. For example, grayscale digital masks were used in a two-step sequential printing process for a hepatic model application. First, a layer of human-induced pluripotent stem cell-derived hepatic progenitor cells (hiPSC-HPCs) was created, supported by a printed lobule structure using 5% (w/v) gelatin methacrylate (GelMA). Then, a second complementary layer of supporting cells (non-parenchymal cells from endothelial and mesenchymal origins in the liver) was added, supported by a vasculature structure printed using 2.5% (w/v) GelMA with 1% (w/v) glycidyl methacrylate-hyaluronic acid.^[171] This innovative approach efficiently produced a 3D *in vitro* hepatic model (**Figure 6A**) that closely mimics the *in vivo* hepatic structure. Over weeks of *in vitro* culturing, this 3D-printed vascularized hepatic model demonstrated phenotypic and functional improvements in the hiPSC-HPCs,^[171] which is a crucial development for the creation of personalized platforms for *in vitro* drug screening and disease studies.

In addition to creating *in vitro* models, one of the most valuable applications of grayscale exposure in biology is the ability to manipulate extracellular matrix (ECM) properties. This manipulation enables researchers to explore the effects of dynamic

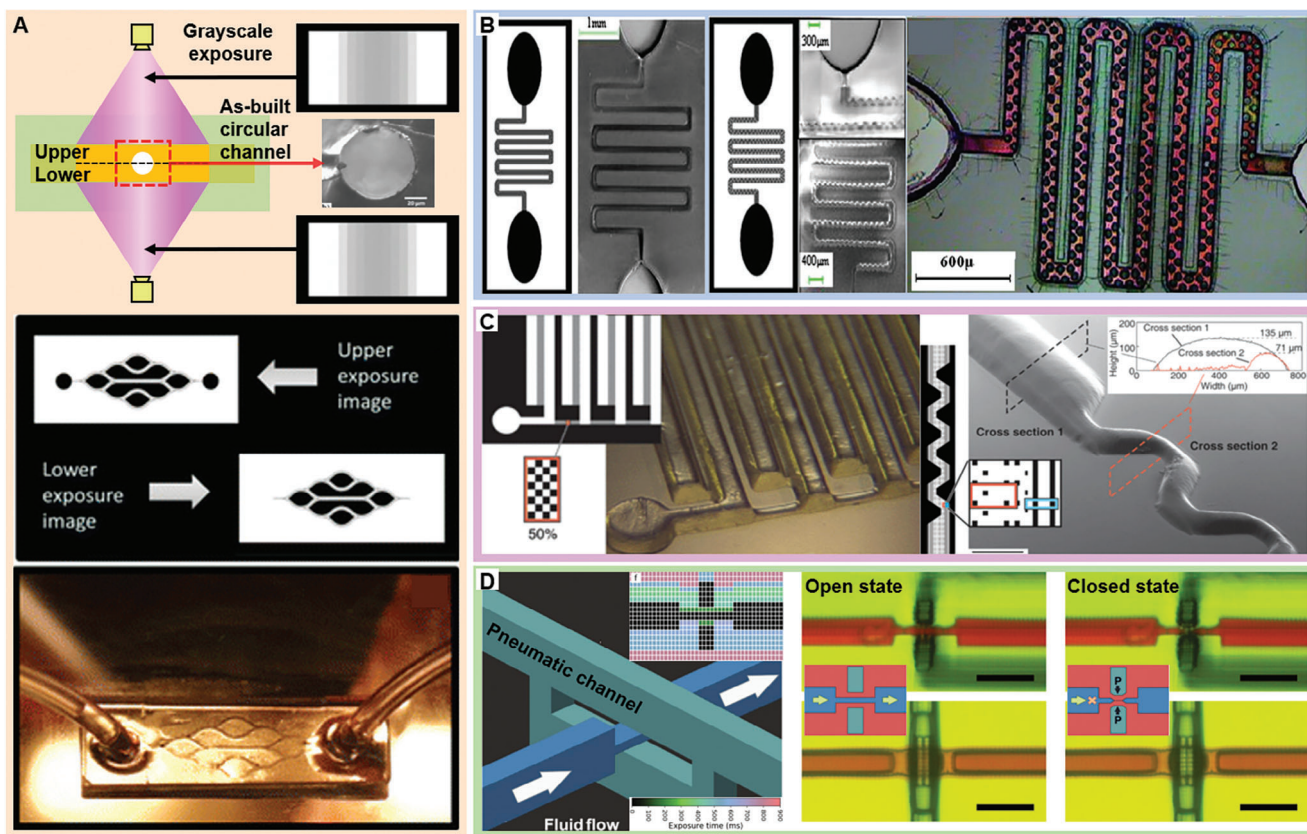


Figure 4. Grayscale vat-photopolymerization in microfluidics. A) Grayscale dual-projection for fabricating circular microfluidic channels. Reproduced with permission.^[161] Copyright 2017, Springer Nature. B) One-step grayscale lithography: grayscale masks and corresponding fabricated microfluidics. Reproduced with permission.^[162] Copyright 2011, Elsevier. C) Multilevel microchannel network with varying widths and heights (left) and curved surfaces (right), generated using grayscale patterns (binary opaque/transparent pixels). Reproduced with permission.^[138] Copyright 2007, Royal Society of Chemistry. D) 3D printing of a squeeze valve by assigning different exposure times per pixel (insets, from left to right: grayscale pattern, schematic diagram of open state, schematic diagram of closed state). Reproduced with permission.^[105] Copyright 2021, Springer Nature.

changes in cell response and direct cell phenotypes. For example, Kloxin et al. developed photodegradable poly(ethylene glycol) (PEG)-based hydrogels that undergo controlled degradation upon light irradiation.^[172] They used these dynamic systems as cell culture platforms with variable elasticity to study the impact of ECM elasticity (ranging from 32 to 7 kPa after 300 s of irradiation) on the fibroblast-myofibroblast differentiation process. After culturing valvular interstitial cells (VICs) on the modulus-gradient hydrogels, they observed modest expression of alpha-smooth muscle actin (α SMA) on both substrates during the initial two days. However, by the third day, there was a notable increase in the organization of α SMA stress fibers on the high-modulus substrates (Figure 6B), which confirmed that low-modulus substrates restrict VIC activation. Yin et al. changed the stiffness in 3D-printed microstructures by adjusting the UV dose in different zones. When bovine pulmonary artery smooth muscle cells were seeded at high density on a fully stiff tube, they uniformly migrated along the wall and formed 3D cell layers encompassing the stiff tube's outer and inner walls, resulting in a 3D vascular tube-like tissue structure (Figure 6C, upper). In contrast, when seeded on a tube with both stiff and soft regions, the cells predominantly migrated along the stiff regions of the wall, creating a 3D half-vascular tube-like tissue structure (Figure 6C, lower).

4.3. Gradient-Color Printing and QR Pattern

Because it offers precise spatial control over the exposure dose, the grayscale approach empowers the printing of gradient-color products and quick response (QR) codes through processes such as photocross-linking,^[26,28,31,154] photodegradation,^[173] or photocatalysis.^[144] These capabilities have the potential for advanced displays, encryption, and anti-counterfeiting applications.

For example, a photocurable resin (ethoxylated trimethylolpropane triacrylate mixed with photoinitiator) was systematically cross-linked at various densities by employing multilevel UV exposure, resulting in a graded polymer in which the cross-linking density affects how much spiropyran (a photochromic functional material) can be absorbed into different areas. This method facilitated the creation of gradient micropatterns because areas subjected to lower UV dosage (characterized by lower cross-linking degree) absorbed more spiropyran, thereby appearing as a darker purple color, whereas areas with higher UV exposure exhibited the opposite effect.^[154] Similarly, fluorescein has been used in gradient-color printing owing to its grayscale-dependent diffusivity: lower cross-linking degree results in higher fluorescein diffusivity and greater color brightness. This innovative approach yields a micropatterned polymer

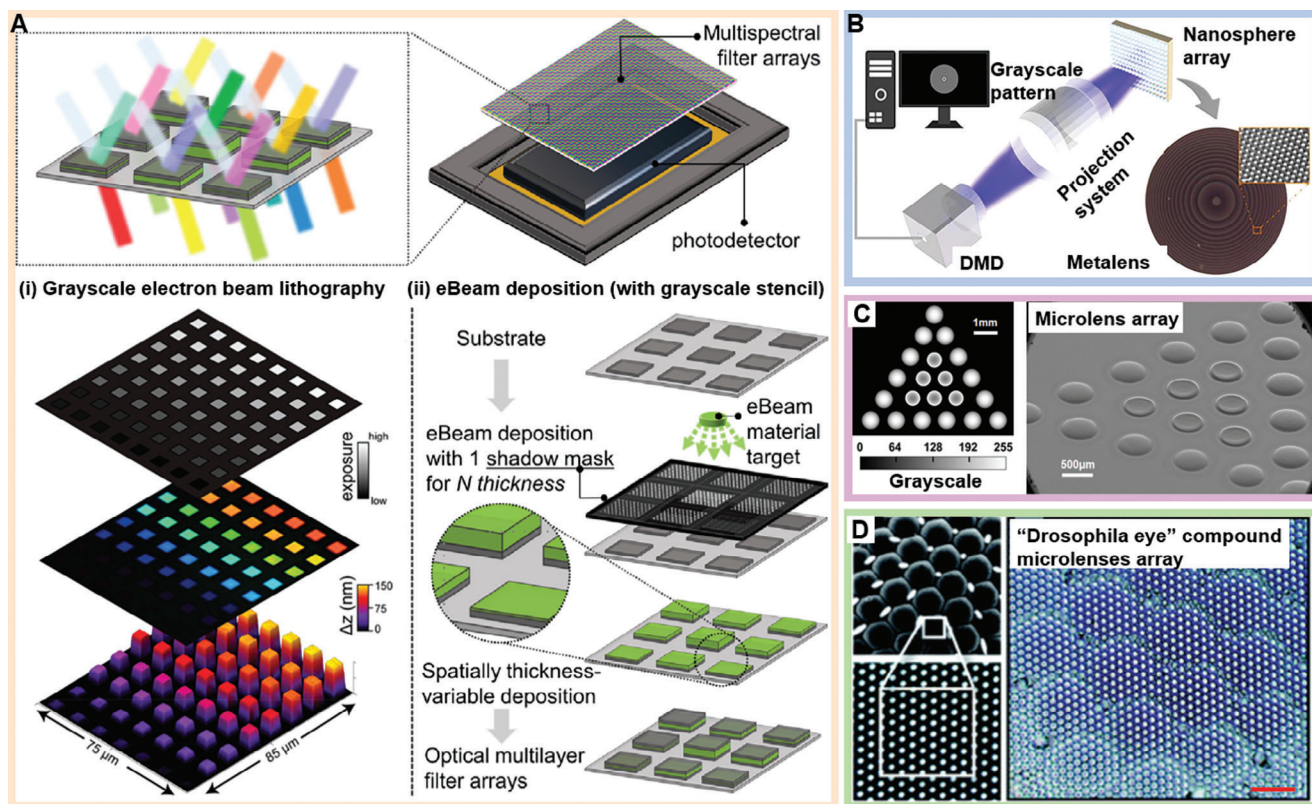


Figure 5. Grayscale patterning in micro-optics. A) Multispectral filter arrays manufactured via i) grayscale electron beam lithography and ii) grayscale stencil-assisted electron beam deposition. Image i) Reproduced with permission.^[168] Copyright 2019, American Chemical Society. Image ii) Reproduced with permission.^[169] Copyright 2020, Optica Publishing Group. B) Metalens fabricated by modulating exposure dosage with the grayscale pattern. Reproduced with permission.^[170] Copyright 2021, American Chemical Society. C) A microlens array printed using an 8-bit pattern. Reproduced with permission.^[165] Copyright 2019, American Chemical Society. D) A bio-inspired grayscale mask (drosophila eye used as an exposure pattern through a high-contrast mask) used to produce micropatterns composed of high-curvature elements with various geometries. Reproduced with permission.^[167] Copyright 2011, Royal Society of Chemistry.

surface with two distinct dye levels, resulting in a scannable QR code.^[26]

Qi et al. recently achieved highly efficient multicolor 3D printing in a single-vat, single-batch process using a diamino-substituted anthraquinone-based dye known as Solvent Blue 104 (Figure 7A).^[28] Their success hinged on their precise control of light exposure. Through modulation of the UV light dose at the pixel level, the printer exerted local control over the concentration of free radicals, consequently influencing the degree of dye oxidation mediated by these free radicals. This level of control allowed for the realization of multicolor 3D printing because the color of Solvent Blue 104 changed in response to the degree of oxidation (a low dose resulted in low oxidation and a blue hue, whereas a high dose led to high oxidation and a yellow hue).

Grayscale photodegradation provides another avenue for achieving gradient-color printing, primarily through photocleavable or photodegradable hydrogels.^[172–174] As an illustrative example, an original grayscale mask was derived from Vincent van Gogh’s painting *The Starry Night*. This mask inverted the tonal values to generate a “negative” projection pattern, which was subsequently projected onto the hydrogels containing photodegradable PEG 4000 4-(3-(acryloyloxymethyl)–2-nitrobenzyloxy)–4-oxobutanoate macromer and non-degradable PEG 4000 diacry-

late. The lightest regions within the “negative” projection pattern corresponded to the most extensively exposed areas, resulting in the highest degree of degradation and thereby the darkest regions in the degraded hydrogel (Figure 7B).

Grayscale exposure technology has also been used to precisely control the photocatalyzed reduction of silver ions in both temporal and spatial domains, thereby allowing the rapid production of plasmonic substrates with customized multiscale structures, ideal for direct color printing.^[144] By adjusting the exposure dosage, silver ions within a TiO₂-capped quartz substrate are reduced to form silver nanoparticles (AgNPs) with varying sizes, each exhibiting distinct colors owing to Fano resonance, resulting in a color image of a campus building (Figure 7C). The spectral dip in this reflection spectrum can be fine-tuned by altering the dimensions of the AgNPs, thus facilitating the generation of plasmonic colors.^[144,175]

4.4. Soft Robotics and the Art of Origami

Grayscale photopolymerization has also been used to control the local properties of materials to induce changes in shape or functionality over time, resulting in “4D printing”.^[143,176–178]

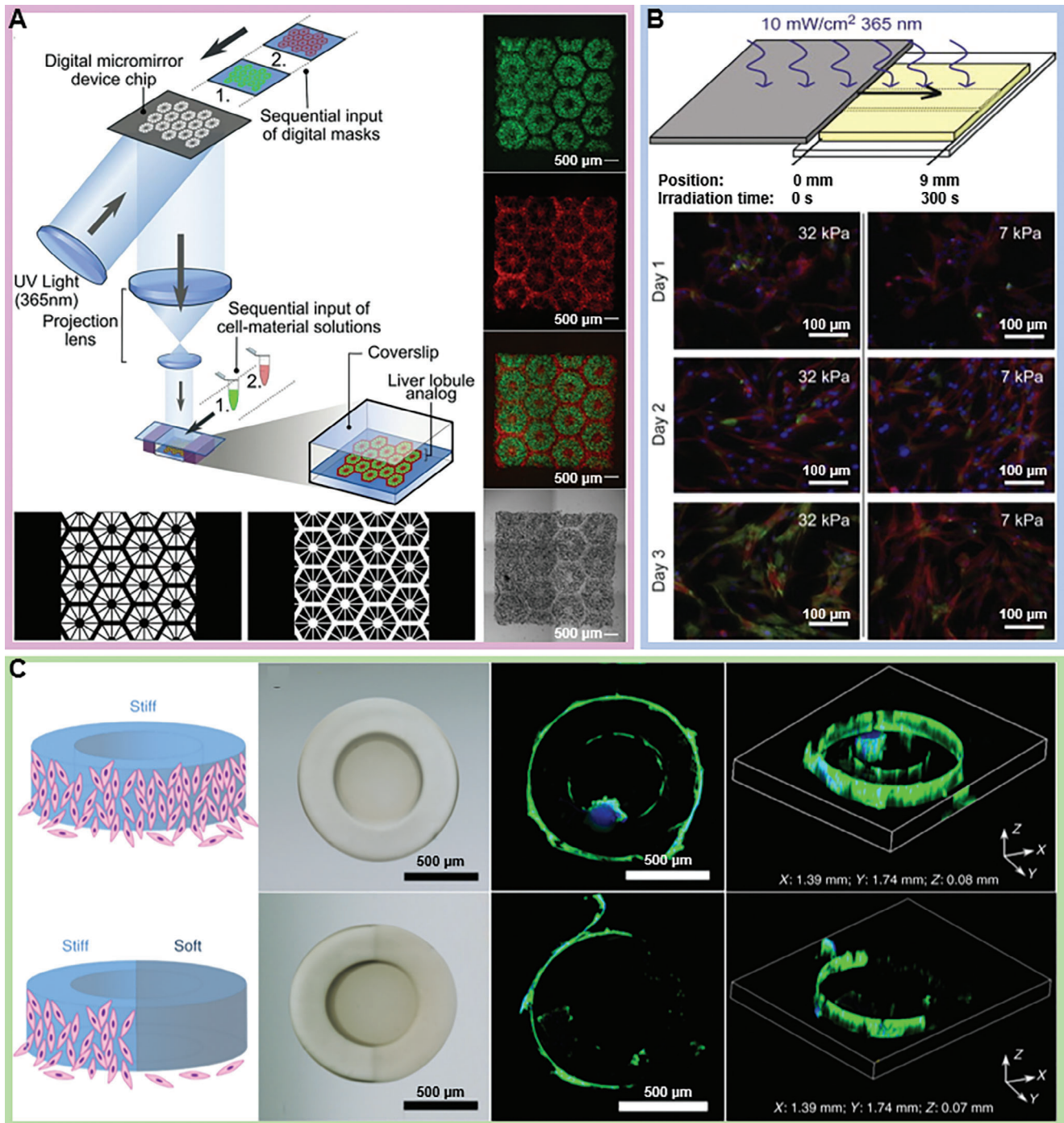


Figure 6. Grayscale vat-photopolymerization in biomedical applications. A) Schematic representation of two-step bioprinting of polymerized lobule (left grayscale digital mask) and vascular (right grayscale digital mask) structures. The images captured under fluorescent and bright field channels reveal patterns of fluorescently labeled hiPSC-HPCs (green) in 5% (w/v) GelMA and supporting cells (red) in 2.5% (w/v) GelMA with 1% GMHA on day 0. hiPSC-HPCs: human-induced pluripotent stem cell-derived hepatic progenitor cells; GelMA: gelatin methacrylate; GMHA: glycidyl methacrylate-hyaluronic acid. Reproduced with permission.^[171] Copyright 2016, National Academy of Sciences. B) Sliding mask used to create a linear exposure gradient across the sample, resulting in a modulus gradient from left to right. To confirm the promotion or suppression of differentiation on the two modulus extremes ($E = 32$ and 7 kPa), VICs were seeded on discrete high- and low-modulus samples. On days 1 and 2, some diffuse α SMA was present but not organized. However, by day 3, organized α SMA stress fibers were prominently observed on high-modulus samples, with limited α SMA present on low-modulus samples. VICs: valvular interstitial cells; α SMA: alpha-smooth muscle actin. Reproduced with permission.^[172] Copyright 2010, Elsevier. C) Spatial control of cellular organization on structures with independently programmed stiffness (stiff: cross-linked at $72 \text{ mJ}/\text{cm}^2$, with $E = 11$ kPa; soft: cross-linked at $44 \text{ mJ}/\text{cm}^2$, with $E = 5$ kPa). Compared to the stiff tube (upper), bovine pulmonary artery smooth muscle cells cultured on grayscale-printed structures (lower) preferred migrating up and attaching to stiff regions over attaching to soft regions. Reproduced with permission.^[94] Copyright 2018, Springer Nature.

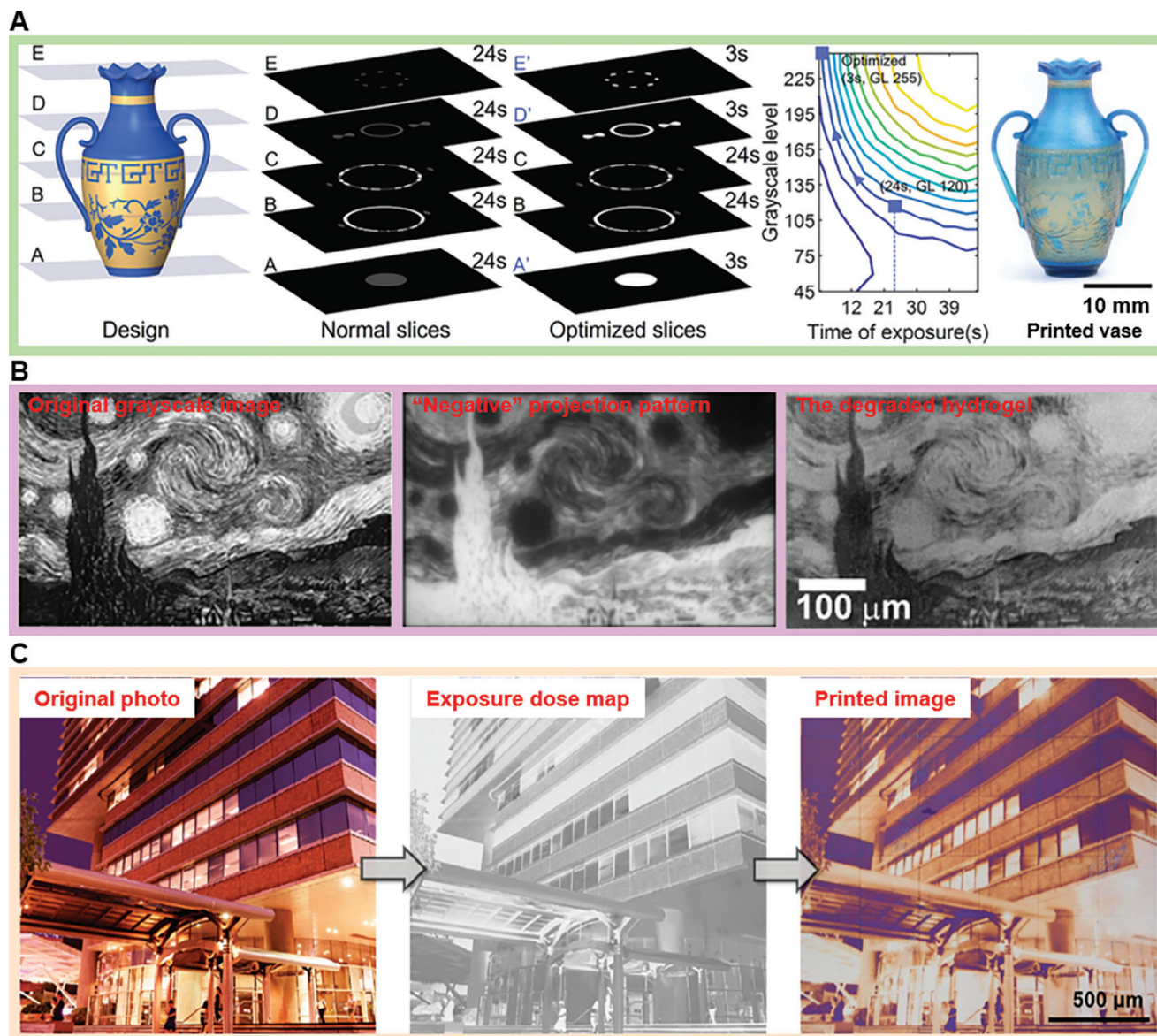


Figure 7. Gradient-color 2D patterns and 3D parts fabricated through grayscale photoreactions. A) An intricately colored vase featuring artistic patterns and characters crafted using grayscale 3D printing. The color of anthraquinone-based dye Solvent Blue 104 transitions from blue to yellow as the light dose and radical concentration increase. Reproduced with permission.^[28] Copyright 2022, Wiley-VCH. B) Fabrication of hydrogel with grayscale degradation. Areas exposed to higher UV dosages (light areas, center panel) exhibited greater degradation of the hydrogels, resulting in darker coloration (right panel). Reproduced with permission.^[173] Copyright 2016, American Chemical Society. C) Direct plasmonic color printing through a grayscale photocatalyzed reaction. The color can be tuned to light yellow, yellow, purple, or red-purple, depending on the exposure dose. Reproduced with permission.^[144] Copyright 2018, American Chemical Society.

Typically, reversible shape-shifting is accomplished through anisotropic responses to specific stimuli (stimuli-responsive hydrogels)^[7,8,179,180] or to swelling/deswelling-induced mismatches (non-responsive hydrogels).^[27,131,180,181]

Stimuli-responsive hydrogels have found extensive use in the development of soft actuators and robots because of their ability to respond to external stimuli such as temperature, pH, ionic concentration, electric fields, or light that result in changes in their degree of swelling.^[180,182] Poly(*N*-isopropylacrylamide) (PNIPAAm), a commonly used monomer for creating thermally responsive hydrogels, has proven to be an ideal material for con-

structing soft actuators and robots.^[7,8,129,179] Han et al. employed grayscale mask-assisted 3D printing to create PNIPAAm microstructures that exhibited reversible shape-shifting responses to temperature changes (Figure 8A).^[7] Using a grayscale mask, they programmed bending behavior into a PNIPAAm microgripper that could open and close in response to low and high temperatures, respectively. Similarly, Hippler et al. used a commercial direct laser writing setup to fabricate PNIPAAm-based hetero-microstructures.^[179] With a constant laser scanning speed of $1 \text{ mm}^{-1}\text{s}$, they fabricated horizontal beams that curved when heated by using a laser at the back focal plane with a power of

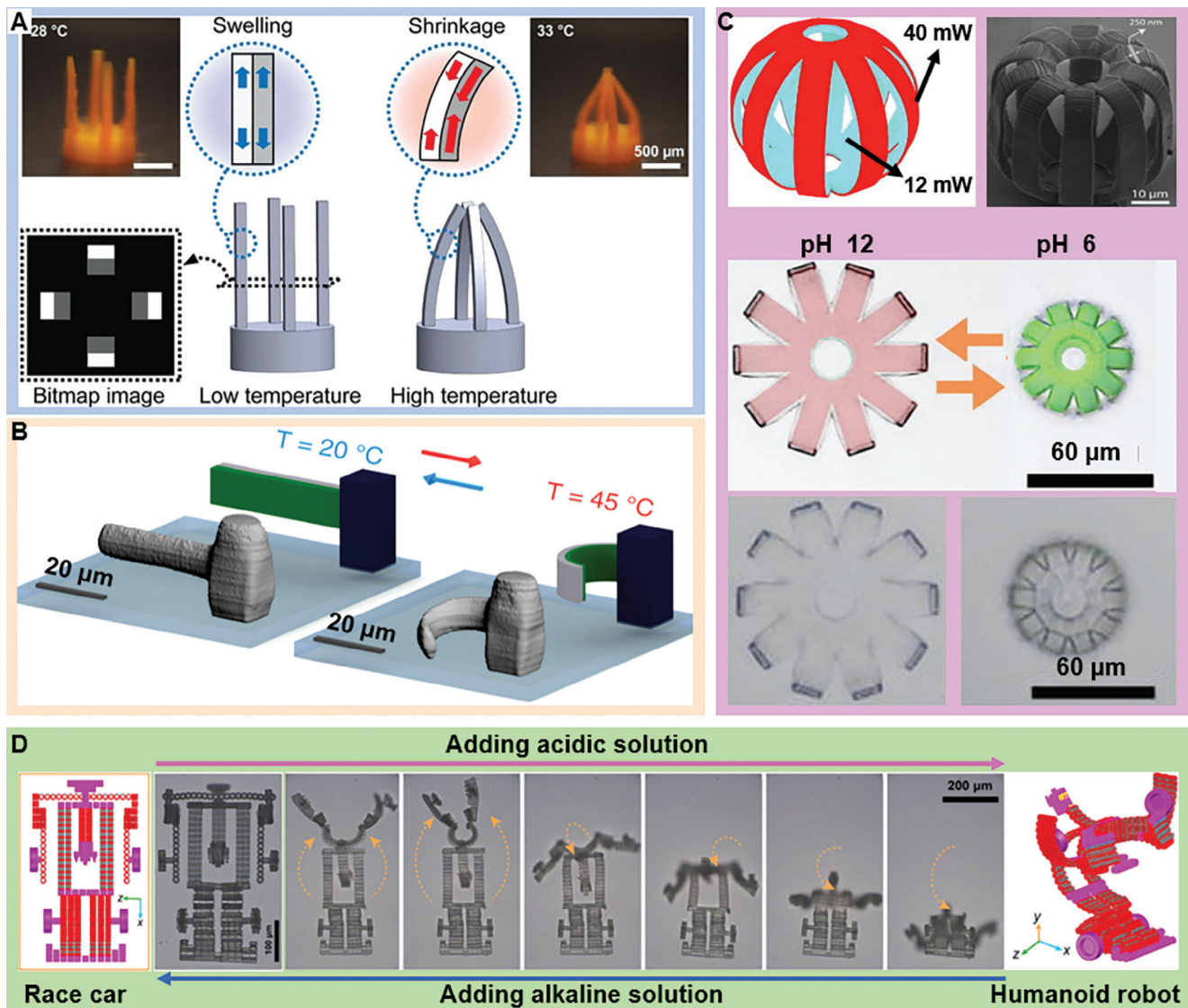


Figure 8. Grayscale vat-photopolymerization in actuators and robots: A,B) achieving shape-shifting through temperature and C,D) pH stimulation. A) Poly(*N*-isopropylacrylamide) (PNIPAAm) microgripper consisting of four beams fabricated using two different grayscale levels. Different swelling ratios between the two regions induce the bending of the beams toward the center at high temperatures (33 °C). Reproduced with permission.^[7] Copyright 2018, Springer Nature. B) Temperature-induced actuator constructed with PNIPAAm-based hetero-microstructures (green: lower laser power; gray: higher power). The horizontal beam started straight at 20 °C but curved at 45 °C. Reproduced with permission.^[179] Copyright 2019, Springer Nature. C) Micro ball structure with increasing cross-linking degree, printed by incrementally raising the laser power from 12 mW (inner layer) to 40 mW (outer layer). When subjected to variations in environmental pH, the micro ball underwent reversible shape transformations, transitioning between a spherical structure (in the swelling state, pH 12) and a slender cylinder (in the shrinking state, pH 6). Reproduced with permission.^[8] Copyright 2020, Elsevier. D) 3D-to-3D shape-morphing process of a microscale transformer from a race car to a humanoid robot (the sample was printed via grayscale direct laser writing). Reproduced with permission.^[129] Copyright 2020, American Association for the Advancement of Science.

30 and 37.5 mW for less and more cross-linking, respectively. These horizontal beams initially remained straight at a temperature of 20 °C but curved at 45 °C (Figure 8B); the response was entirely reversible and free from any degradation.

In the same year, Duan et al. developed stimulus-responsive hydrogels and used them to print microstructures featuring graded cross-linking densities, which exhibited significant responses to alterations in both temperature and pH.^[8,129] For example, they printed a micro ball (Figure 8C) by varying the laser power from 12 mW (for the inner layer) to 40 mW (for the outer

layer). This structure could transition between a spherical form (swelling state, pH 12) and a slender cylinder (shrinking state, pH 6). In addition, they demonstrated the ability of a one-step direct laser writing process to create a microscale transformer using carefully formulated stimulus-responsive hydrogels.^[129] When exposed to different solutions (acidic or alkaline), this 3D-printed transformer could undergo shape transformations between that of a race car and a humanoid robot (Figure 8D).

Owing to the limited availability of stimuli-responsive hydrogels, researchers have explored the potential of non-responsive

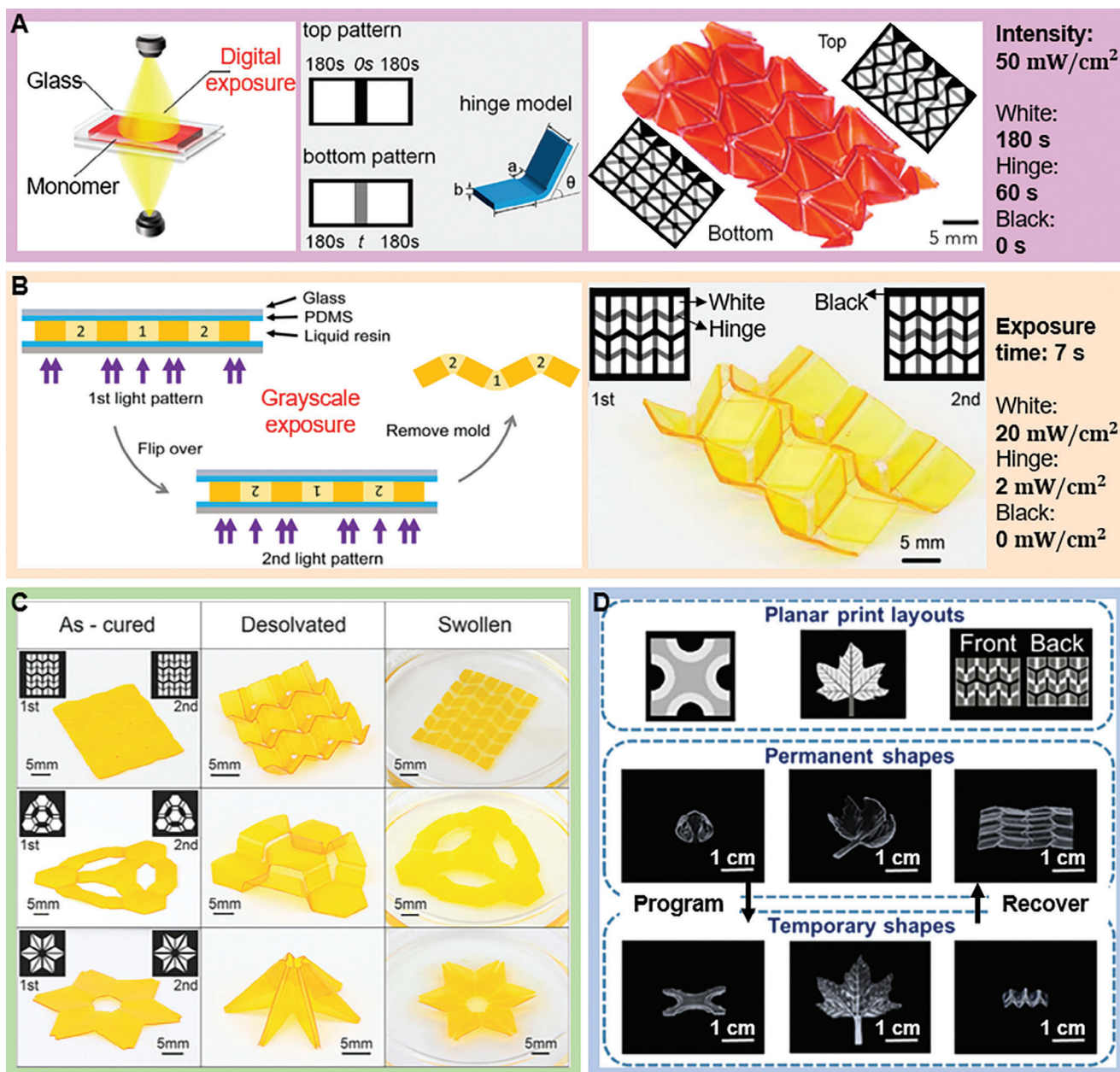


Figure 9. Grayscale vat-photopolymerization for origami fabrication. A) Creation of origami through controlled exposure times. Reproduced with permission.^[143] Copyright 2020, Elsevier. B) Origami production via light intensity modulation. Reproduced with permission.^[27] Copyright 2017, American Association for the Advancement of Science. C) Origami creation using grayscale exposure, with shape transformation achieved through solvent treatment (acetone absorption and drying; insets in the first column depict two grayscale patterns for printing). Adapted with permission.^[106] Copyright 2017, Wiley-VCH. D) Origami fabrication through digital exposure, with shape memory behavior controlled by temperature programming (in the planar print layouts, the black background signifies no light exposure; light and dark regions correspond to light exposures of 14 and 30 s, respectively). Reproduced with permission.^[149] Copyright 2019, American Chemical Society.

hydrogels to exhibit swelling characteristics in a solvent medium. These hydrogels can de-swell when dried or adjust their swelling degree depending on the surrounding medium. This exploration has promoted the development of origami structures, grippers, and sensors specifically engineered to adapt to various solvent environments.^[27,106,112,131,180,181,183]

Multiple research groups have harnessed FPP-based techniques for crafting 3D origami structures. In-plane variations of

light intensity have been achieved by using grayscale masks or digital exposure; the light intensity across the thickness direction is controlled through light attenuation (based on the Lambert-Beer law), thereby resulting in local regions with graded degrees of cross-linking.^[106] Xie et al. used a double-sided illumination technique, adjusting the light dose by varying the exposure time, to fabricate a Miura structure (Figure 9A).^[143] Qi et al., in comparison, created a similar origami structure by employing a

two-side illumination setup to regulate the light dose using grayscale masks (Figure 9B).^[27] Select grayscale-printed origami structures can transition into flat shapes when immersed in acetone. Subsequently, these flat sheets return to their original origami configurations upon removal from the acetone bath (Figure 9C).

Akin to the non-responsive hydrogel, a temperature-responsive hydrogel has been prepared that manifests reversible deformation characteristics in response to temperature alterations (Figure 9D). The cycles of unfolding at 70 °C and folding at 10 °C were repeatable. However, it is worth noting that the response times to temperature stimuli^[149] (unfolding, folding: >2 min) were longer compared with those observed in solvent hydrogels^[106] (unfolding: 10–30 s; folding: 2 min). This capacity for reversible shape-shifting, whether through the repeated absorption and evaporation of acetone or low/high-temperature switching, holds significant promise for developing shape-shifting 3D nano-phonic devices and electronics.^[27,106,149]

5. Conclusion and Perspectives

Grayscale photopolymerization 3D printing surpasses traditional VP techniques when fabricating complex structures with gradient properties. This discussion examined and compared various grayscale methods for controlling light exposure and material properties. Grayscale mask-assisted 3D printing has become mainstream because of its fabrication speed and scalability advantages. However, grayscale TPP is the superior choice when exceptionally high-resolution gradients are required.

Despite the recent successes of various grayscale 3D printing methods, improvements are still needed. Volumetric 3D printing, a technology introduced in 2019, is still in its developmental stages and faces numerous challenges, such as formulation limitation and scalability issues in xolography, and dose distribution and light scattering issues in CAL. These challenges must be addressed before volumetric printing can be effectively employed for true grayscale printing. Furthermore, although there has been significant progress in serial (TPP) and planar (projection-based) grayscale 3D printing, limitations such as feedstock options and fabrication time in the TPP technique, as well as resolution and bitmap optimization in projection-based methods, still need to be overcome.

5.1. Improvements in Feedstocks

Because VP is a light-based technique, the requirement for transparency limits the possibility of expanding the available material set by loading the resin bath with particles of high refractive index (e.g., ceramics or metals with refractive index >2).^[88] This inherent limitation extends to the choice of materials for grayscale SLA: current grayscale VP 3D printing primarily uses single transparent photoreins instead of particle-loaded composite formulations. In the near future, developing photocurable composite formulations for grayscale VP and reducing scattering effects in composite feedstocks will be necessary. The ability to freely choose fillers (e.g., polymers, ceramics) presents opportunities to incorporate additional functionalities, such as

biomineralization^[184,185] and extended responsive features,^[112] into 3D-printed components. Beyond composite grayscale 3D printing, combining multiple materials with grayscale VP offers a promising avenue for enhancing the multifunctionality of 3D printing.^[171,186] Multi-material grayscale 3D printing could facilitate the creation of FGMs in various orientations, leveraging heterogeneous structures or ingredients to produce 3D-printed components (e.g., soft robots and actuators) with added anisotropic functionalities. It is envisioned that differently graded composites will be manufactured and assembled using various parallel modules to construct complete and functional devices.^[187,188]

5.2. Improvements in Grayscale Methods

As mentioned previously, the predominant grayscale VP method is the grayscale mask-assisted 3D printing, typically employing 8-bit patterns that yield varying UV light intensities during printing. Because many projection-based printers are designed for black-and-white 2D slices, supplementary binary grayscale masks are required. These masks can be generated using different pixel-coding algorithms. The emergence of digital halftoning SLA has inspired the development of coding techniques for generating binary grayscale masks, but only a few instances of such halftoning approaches appear in the literature.^[136–138,141,189,190] Significant challenges remain. In binary grayscale masks, the number and size of pixels per unit area are critical factors in determining the level of discretization or continuity in the transferred topographies and the quality of transitions between different brightness levels.^[137] In addition, the balance between resolution and efficiency is crucial for manufacturing high-resolution graded materials. The success of halftoning printing hinges on factors like light scattering and the diffusion of activated photoinitiators from illuminated to non-illuminated regions, which partially solidify the material. However, light scattering and activated photoinitiator diffusion broaden the effective exposure region of each “ON” pixel, thus deteriorating the print resolution.^[141] Therefore, the design and optimization of projection patterns are crucial for the successful execution of grayscale 3D printing.

Additional research is needed to assess the material properties achieved through different grayscale methods. In situations where minimizing surface roughness is crucial, such as sloped arch structures^[137] and optical elements,^[40] an 8-bit pattern that can offer nearly continuous variations in light intensity during exposure would be the superior choice. Conversely, for applications like microfluidics, where certain mixer channels benefit from rough surfaces to enhance mixing efficiency,^[163] halftoning-based grayscale 3D printing would be the preferred method.

5.3. Extending Grayscale VP to Other Engineering and Biomedical Applications

Because most current research in grayscale VP 3D printing primarily concentrates on fabricating materials with graded properties (e.g., mechanical, thermal, optical, and swelling characteristics) through variations in cross-linking degree within the pure resin, there remains a need for further exploration in engineering applications (e.g., porous electrical pathways,^[191] magnetic

devices^[192]). Composite and multi-material grayscale 3D printing methods may offer solutions to address these challenges. In addition, most current studies for biomedical applications have focused on fabricating anisotropic substrates or in vitro models for cell culturing. There is room for investigation into a broader spectrum of emerging applications, such as bioimplants, organoids, and organ-on-a-chip systems, presenting exciting prospects for grayscale 3D printing.^[193]

Over the last two decades, considerable progress has been made in grayscale VP 3D printing technologies. However, to further advance gradient fabrication for emerging applications such as bioimplants, organs-on-chips, and electrical/magnetic devices, it will be essential to coordinate efforts in developing new methods for grayscale mask generation, photocurable composites, and multi-material formulations. Multidisciplinary research and collaborations between academia and industry will likely be crucial in extending this technology.

Acknowledgements

G.F. acknowledges KU Leuven for the funding of a postdoctoral mandate (PDMT2/22/050). The authors acknowledge KU Leuven for funding research projects IDN/20/016 and C3/21/027.

Conflict of Interest

The authors declare no conflict of interest.

Keywords

functionally graded materials, grayscale 3D printing, photopolymerization

- [1] M. Naebe, K. Shirvanimoghaddam, *Appl. Mater. Today* **2016**, *5*, 223.
- [2] M. Sai Charan, A. K. Naik, N. Kota, T. Laha, S. Roy, *Int. Mater. Rev.* **2022**, *67*, 797.
- [3] J. Chen, X. Liu, Y. Tian, W. Zhu, C. Yan, Y. Shi, L. B. Kong, H. J. Qi, K. Zhou, *Adv. Mater.* **2022**, *34*, 2102877.
- [4] G. H. Loh, E. Pei, D. Harrison, M. D. Monzón, *Addit. Manuf.* **2018**, *23*, 34.
- [5] M. Koizumi, *Compos. Part B Eng.* **1997**, *28*, 1.
- [6] N. W. Bartlett, M. T. Tolley, J. T. B. Overvelde, J. C. Weaver, B. Mosaddegh, K. Bertoldi, G. M. Whitesides, R. J. Wood, *Science* **2015**, *349*, 161.
- [7] D. Han, Z. Lu, S. A. Chester, H. Lee, *Sci. Rep.* **2018**, *8*, 1963.
- [8] D. Jin, Q. Chen, T. Y. Huang, J. Huang, L. Zhang, H. Duan, *Mater. Today* **2020**, *32*, 19.
- [9] M. Wang, W. Li, L. S. Mille, T. Ching, Z. Luo, G. Tang, C. E. Garciamendez, A. Lesha, M. Hashimoto, Y. S. Zhang, *Adv. Mater.* **2022**, *34*, 2107038.
- [10] C. Petit, L. Montanaro, P. Palmero, *Int. J. Appl. Ceram. Technol.* **2018**, *15*, 820.
- [11] F. Xu, X. Zhang, H. Zhang, *Eng. Struct.* **2018**, *171*, 309.
- [12] E. Müller, Č. Drašar, J. Schilz, W. Kaysser, *Mater. Sci. Eng. A* **2003**, *362*, 17.
- [13] K. B. Ghosh, J. Mukhopadhyay, R. N. Basu, *J. Power Sources* **2016**, *328*, 15.
- [14] S. P. Parida, P. Charan Jena, *Mater. Today Proc* **2019**, *18*, 2942.
- [15] H. Ravanbakhsh, V. Karamzadeh, G. Bao, L. Mongeau, D. Juncker, Y. S. Zhang, *Adv. Mater.* **2021**, *33*, 2104730.
- [16] C. Parra-Cabrera, C. Achille, S. Kuhn, R. Ameloot, *Chem. Soc. Rev.* **2018**, *47*, 209.
- [17] A. K. Au, W. Huynh, L. F. Horowitz, A. Folch, *Angew. Chem., Int. Ed.* **2016**, *55*, 3862.
- [18] A. Ambrosi, M. Pumera, *Chem. Soc. Rev.* **2016**, *45*, 2740.
- [19] F. Zhang, M. Wei, V. V. Viswanathan, B. Swart, Y. Shao, G. Wu, C. Zhou, *Nano Energy* **2017**, *40*, 418.
- [20] N. Bhattacharjee, A. Urrios, S. Kang, A. Folch, *Lab Chip* **2016**, *16*, 1720.
- [21] A. Naderi, N. Bhattacharjee, A. Folch, *Annu. Rev. Biomed. Eng.* **2019**, *21*, 325.
- [22] L. Yue, S. Macrae Montgomery, X. Sun, L. Yu, Y. Song, T. Nomura, M. Tanaka, H. Jerry Qi, *Nat. Commun.* **2023**, *14*, 1251.
- [23] J. R. Tumbleston, D. Shirvanyants, N. Ermoshkin, R. Januszewicz, A. R. Johnson, D. Kelly, K. Chen, R. Pinschmidt, J. P. Rolland, A. Ermoshkin, E. T. Samulski, J. M. DeSimone, *Science (80-)*. **2015**, *347*, 1349.
- [24] S. N. Sanders, T. H. Schloemer, M. K. Gangishetty, D. Anderson, M. Seitz, A. O. Gallegos, R. C. Stokes, D. N. Congreve, *Nature* **2022**, *604*, 474.
- [25] M. Regehy, Y. Garmshausen, M. Reuter, N. F. König, E. Israel, D. P. Kelly, C. Chou, K. Koch, B. Asfari, S. Hecht, *Nature* **2020**, *588*, 620.
- [26] X. Kuang, J. Wu, K. Chen, Z. Zhao, Z. Ding, F. Hu, D. Fang, H. J. Qi, *Sci. Adv.* **2019**, *5*, eaav5790.
- [27] Z. Zhao, J. Wu, X. Mu, H. Chen, H. J. Qi, D. Fang, *Sci. Adv.* **2017**, *3*, e1602326.
- [28] X. Peng, L. Yue, S. Liang, S. Montgomery, C. Lu, C. M. Cheng, R. Beyah, R. R. Zhao, H. J. Qi, *Adv. Funct. Mater.* **2022**, *32*, 2112329.
- [29] D. G. Moore, L. Barbera, K. Masania, A. R. Studart, *Nat. Mater.* **2020**, *19*, 212.
- [30] G. I. Peterson, J. J. Schwartz, D. Zhang, B. M. Weiss, M. A. Ganter, D. W. Storti, A. J. Boydston, *ACS Appl. Mater. Interfaces* **2016**, *8*, 29037.
- [31] P. Jiang, C. Yan, Z. Ji, Y. Guo, X. Zhang, X. Jia, X. Wang, F. Zhou, *ACS Appl. Mater. Interfaces* **2019**, *11*, 42586.
- [32] P. Jiang, Y. Zhang, X. Mu, D. Liu, Y. Liu, R. Guo, Z. Ji, X. Wang, X. Wang, *Adv. Mater. Technol.* **2022**, *7*, 2101288.
- [33] C. W. Hull, Apparatus for Production of Three Dimensional Objects by Stereolithography, **1986**.
- [34] C. Chatwin, M. Farsari, S. Huang, M. Heywood, P. Birch, R. Young, J. Richardson, *Appl. Opt.* **1998**, *37*, 7514.
- [35] G. Fei, T. Wei, Q. Shi, Y. Guo, H. Oprins, S. Yang, *Solid Free. Fabr. 2019: Proc. 30th Annu. Int. Solid Free. Fabr. Symp.* **2019**, *30*, 2028.
- [36] N. A. Rodriguez, H. Song, M. Chen, J. S. Oakdale, E. B. Duoss, C. C. Seepersad, R. H. Crawford, *Addit. Manuf.* **2022**, *52*, 102641.
- [37] C. Sun, N. Fang, D. M. Wu, X. Zhang, *Sensors Actuators A Phys* **2005**, *121*, 113.
- [38] H. Zhao, J. Sha, X. Wang, Y. Jiang, T. Chen, T. Wu, X. Chen, H. Ji, Y. Gao, L. Xie, Y. Ma, *Lab Chip* **2019**, *19*, 2651.
- [39] X. Zheng, J. Deotte, M. P. Alonso, G. R. Farquar, T. H. Weisgraber, S. Gemberling, H. Lee, N. Fang, C. M. Spadaccini, *Rev. Sci. Instrum.* **2012**, *83*, 125001.
- [40] X. Chen, W. Liu, B. Dong, J. Lee, H. O. T. Ware, H. F. Zhang, C. Sun, *Adv. Mater.* **2018**, *30*, 1705683.
- [41] H. H. Hwang, W. Zhu, G. Victorine, N. Lawrence, S. Chen, *Small Methods* **2018**, *2*, 1700277.
- [42] Y. Wang, D. Xue, D. Mei, *J. Manuf. Sci. Eng.* **2020**, *142*, 021003.
- [43] D. A. Walker, J. L. Hedrick, C. A. Mirkin, *Science (80-)*. **2019**, *366*, 360.
- [44] B. E. Kelly, I. Bhattacharya, H. Heidari, M. Shusteff, C. M. Spadaccini, H. K. Taylor, *Science (80-)*. **2019**, *363*, 1075.
- [45] J. T. Toombs, M. Luitz, C. C. Cook, S. Jenne, C. C. Li, B. E. Rapp, F. Kotz-Helmer, H. K. Taylor, *Science* **2022**, *376*, 308.

- [46] M. Shusteff, A. E. M. Browar, B. E. Kelly, J. Henriksson, T. H. Weisgraber, R. M. Panas, N. X. Fang, C. M. Spadaccini, *Sci. Adv.* **2017**, *3*, eaao5496.
- [47] D. Loterie, P. Delrot, C. Moser, *Nat. Commun.* **2020**, *11*, 852.
- [48] P. N. Bernal, P. Delrot, D. Loterie, Y. Li, J. Malda, C. Moser, R. Levato, *Adv. Mater.* **2019**, *31*, 1904209.
- [49] A. Bagheri, J. Jin, *ACS Appl. Polym. Mater.* **2019**, *1*, 593.
- [50] A. M., 'FDM vs. SLA: Compare the Two Most Popular Types of 3D Printers', can be found at: <https://formlabs.com/eu/blog/fdm-vs-sla-compare-types-of-3d-printers/>, **2018** (accessed: April 2024).
- [51] R. L. Truby, J. A. Lewis, *Nature* **2016**, *540*, 371.
- [52] L. Valot, J. Martinez, A. Mehdi, G. Subra, *Chem. Soc. Rev.* **2019**, *48*, 4049.
- [53] F. Mayer, D. Ryklin, I. Wacker, R. Curticean, M. Čalkovský, A. Niemeyer, Z. Dong, P. A. Levkin, D. Gerthsen, R. R. Schröder, M. Wegener, *Adv. Mater.* **2020**, *32*, 2002044.
- [54] S. K. Saha, D. Wang, V. H. Nguyen, Y. Chang, J. S. Oakdale, S. C. Chen, *Science* **2019**, *366*, 105.
- [55] Q. Geng, D. Wang, P. Chen, S. C. Chen, *Nat. Commun.* **2019**, *10*, 2179.
- [56] C. Maibohm, O. F. Silvestre, J. Borme, M. Sinou, K. Heggarty, J. B. Nieder, *Sci. Rep.* **2020**, *10*, 8740.
- [57] J. Li, M. Pumera, *Chem. Soc. Rev.* **2021**, *50*, 2794.
- [58] W. Zhu, J. Li, Y. J. Leong, I. Rozen, X. Qu, R. Dong, Z. Wu, W. Gao, P. H. Chung, J. Wang, S. Chen, *Adv. Mater.* **2015**, *27*, 4411.
- [59] G. Lipkowitz, T. Samuelsen, K. Hsiao, B. Lee, M. T. Dulay, I. Coates, H. Lin, W. Pan, G. Toth, L. Tate, E. S. G. Shaqfeh, J. M. DeSimone, *Sci. Adv.* **2022**, *8*, 3917.
- [60] B. E. Kelly, I. Bhattacharya, M. Shusteff, H. K. Taylor, C. M. Spadaccini, *Solid Free. Fabr. 2017 Proc. 28th Annu. Int. Solid Free. Fabr. Symp. – An Addit. Manuf. Conf. SFF* **2017**, *2017*, 938.
- [61] M. Chen, M. Zhong, J. A. Johnson, *Chem. Rev.* **2016**, *116*, 10167.
- [62] Q. Michaudel, V. Kottisch, B. P. Fors, *Angew. Chem., Int. Ed.* **2017**, *56*, 9670.
- [63] O. S. Taskin, G. Yilmaz, M. A. Tasdelen, Y. Yagci, *Polym. Int.* **2014**, *63*, 902.
- [64] S. C. Ligon, R. Liska, J. Stampfl, M. Gurr, R. Mülhaupt, *Chem. Rev.* **2017**, *117*, 10212.
- [65] J. V. Crivello, *J. Polym. Sci. Part A Polym. Chem.* **1999**, *37*, 4241.
- [66] P. Bednarczyk, K. Mozelewska, M. Nowak, Z. Czech, *Materials (Basel)* **2021**, *14*, 4150.
- [67] S. M. Schissel, J. L. P. Jessop, *Polymer (Guildf)* **2019**, *161*, 78.
- [68] M. Xiao, Y. He, J. Nie, *Des. Monomers Polym.* **2008**, *11*, 383.
- [69] A. Fantoni, J. Ecker, M. Ahmadi, T. Koch, J. Stampfl, R. Liska, S. Baudis, *ACS Sustainable Chem. Eng.* **2023**, *11*, 12004.
- [70] E. K. U. Larsen, N. B. Larsen, K. Almdal, E. K. U. Larsen, N. B. Larsen, K. Almdal, *J. Polym. Sci. Part B Polym. Phys.* **2016**, *54*, 1195.
- [71] J. J. Schwartz, A. J. Boydston, *Nat. Commun.* **2019**, *10*, 791.
- [72] X. Zhang, W. Xi, S. Huang, K. Long, C. N. Bowman, *Macromolecules* **2017**, *50*, 5652.
- [73] N. D. Dolinski, E. B. Callaway, C. S. Sample, L. F. Gockowski, R. Chavez, Z. A. Page, F. Eisenreich, S. Hecht, M. T. Valentine, F. W. Zok, C. J. Hawker, *ACS Appl. Mater. Interfaces* **2021**, *13*, 22065.
- [74] S. Bialas, L. Michalek, D. E. Marschner, T. Krappitz, M. Wegener, J. Blinco, E. Blasco, H. Frisch, C. Barner-Kowollik, *Adv. Mater.* **2019**, *31*, 1807288.
- [75] V. Kottisch, Q. Michaudel, B. P. Fors, *J. Am. Chem. Soc.* **2017**, *139*, 10665.
- [76] N. D. Dolinski, Z. A. Page, E. B. Callaway, F. Eisenreich, R. V. Garcia, R. Chavez, D. P. Bothman, S. Hecht, F. W. Zok, C. J. Hawker, *Adv. Mater.* **2018**, *30*, 1800364.
- [77] P. Wiroonpochit, K. Uttra, K. Jantawatchai, N. Hansupalak, Y. Chisti, *Ind. Eng. Chem. Res.* **2017**, *56*, 7217.
- [78] Y. Yu, L. Shang, J. Guo, J. Wang, Y. Zhao, *Nat. Protoc.* **2018**, *13*, 2557.
- [79] S. Li, Y. He, J. Nie, *J. Photochem. Photobiol. A Chem.* **2007**, *191*, 25.
- [80] K. J. Schafer, J. M. Hales, M. Balu, K. D. Belfield, E. W. Van Stryland, D. J. Hagan, *J. Photochem. Photobiol. A Chem.* **2004**, *162*, 497.
- [81] A. P. Zhang, X. Qu, P. Soman, K. C. Hribar, J. W. Lee, S. Chen, S. He, *Adv. Mater.* **2012**, *24*, 4266.
- [82] M. Wang, P. Zhang, M. Shamsi, J. L. Thelen, W. Qian, V. K. Truong, J. Ma, J. Hu, M. D. Dickey, *Nat. Mater.* **2022**, *21*, 359.
- [83] J. Wang, T. Lu, M. Yang, D. Sun, Y. Xia, T. Wang, *Sci. Adv.* **2019**, *5*, 8769.
- [84] L. Nie, J. Zhang, Q. Wu, G. Fei, K. Hu, L. Fang, S. Yang, *Mater. Lett.* **2020**, *261*, 127014.
- [85] Z. Wang, R. Abdulla, B. Parker, R. Samanipour, S. Ghosh, K. Kim, *Biofabrication* **2015**, *7*, 045009.
- [86] B. D. Fairbanks, M. P. Schwartz, C. N. Bowman, K. S. Anseth, *Bio-materials* **2009**, *30*, 6702.
- [87] G. Fei, L. Nie, L. Zhong, Q. Shi, K. Hu, C. Parra-Cabrera, H. Oprins, R. Ameloot, S. Yang, *Mater. Today Commun.* **2022**, *31*, 103482.
- [88] G. Fei, C. Parra-Cabrera, K. Zhong, M. L. Tietze, K. Clays, R. Ameloot, *ACS Appl. Polym. Mater.* **2021**, *3*, 6705.
- [89] S. Sung, D. S. Kim, *J. Appl. Polym. Sci.* **2013**, *129*, 1340.
- [90] A. Nojoomi, H. Arslan, K. Lee, K. Yum, *Nat. Commun.* **2018**, *9*, 3705.
- [91] J. Ji, M. Wang, M. Hu, L. Mao, Q. Wang, W. Zhou, M. Tian, J. Yuan, K. Hu, Y. Wei, *Compos. Part B Eng.* **2021**, *206*, 108526.
- [92] H. Ryu, Y. Park, H. Luan, G. Dalgin, K. Jeffris, H. J. Yoon, T. S. Chung, J. U. Kim, S. S. Kwak, G. Lee, H. Jeong, J. Kim, W. Bai, J. Kim, Y. H. Jung, A. K. Tryba, J. W. Song, Y. Huang, L. H. Philipson, J. D. Finan, J. A. Rogers, *Adv. Mater.* **2021**, *33*, 2100026.
- [93] B. Ganster, U. K. Fischer, N. Moszner, R. Liska, *Macromol. Rapid Commun.* **2008**, *29*, 57.
- [94] H. Yin, Y. Ding, Y. Zhai, W. Tan, X. Yin, *Nat. Commun.* **2018**, *9*, 4096.
- [95] Q. L. Zhu, C. F. Dai, D. Wagner, O. Khoruzhenko, W. Hong, J. Brey, Q. Zhang, Z. L. Wu, *Adv. Sci.* **2021**, *5*, 2102353.
- [96] M. A. Tasdelen, M. Ciftci, Y. Yagci, *Macromol. Chem. Phys.* **2012**, *213*, 1391.
- [97] D. Gidon, D. Aydin, S. Kizilel, *Biomed. Mater.* **2015**, *10*, 065001.
- [98] H. Goodarzi Hosseinabadi, E. Dogan, A. K. Miri, L. Ionov, *ACS Biomater. Sci. Eng.* **2022**, *8*, 1381.
- [99] X. Xu, A. Seijo-Rabina, A. Awad, C. Rial, S. Gaisford, A. W. Basit, A. Goyanes, *Int. J. Pharm.* **2021**, *609*, 121199.
- [100] S. Shanmugam, J. Xu, C. Boyer, *J. Am. Chem. Soc.* **2015**, *137*, 9174.
- [101] A. Al Mousawi, C. Poriel, F. Dumur, J. Toufaily, T. Hamieh, J. P. Fouassier, J. Lalevée, *Macromolecules* **2017**, *50*, 746.
- [102] P. Xiao, F. Dumur, B. Graff, J. P. Fouassier, D. Gigmes, J. Lalevée, *Macromolecules* **2013**, *46*, 6744.
- [103] N. Corrigan, J. Xu, C. Boyer, *Macromolecules* **2016**, *49*, 3274.
- [104] S. Shanmugam, J. Xu, C. Boyer, *Angew. Chem., Int. Ed.* **2016**, *55*, 1036.
- [105] J. L. Sanchez Noriega, N. A. Chartrand, J. C. Valdoz, C. G. Cribbs, D. A. Jacobs, D. Poulson, M. S. Viglione, A. T. Woolley, P. M. Van Ry, K. A. Christensen, G. P. Nordin, *Nat. Commun.* **2021**, *12*, 5509.
- [106] Z. Zhao, J. Wu, X. Mu, H. Chen, H. J. Qi, D. Fang, *Macromol. Rapid Commun.* **2017**, *38*, 1600625.
- [107] D. Han, C. Farino, C. Yang, T. Scott, D. Browe, W. Choi, J. W. Freeman, H. Lee, *ACS Appl. Mater. Interfaces* **2018**, *10*, 17512.
- [108] Y. Zhang, Z. Dong, C. Li, H. Du, N. X. Fang, L. Wu, Y. Song, *Nat. Commun.* **2020**, *11*, 1.
- [109] A. Urrios, C. Parra-Cabrera, N. Bhattacharjee, A. M. Gonzalez-Suarez, L. G. Rigat-Brugarolas, U. Nallapatti, J. Samitier, C. A. DeForest, F. Posas, J. L. Garcia-Cordero, A. Folch, *Lab Chip* **2016**, *16*, 2287.
- [110] Q. Ge, A. H. Sakhaei, H. Lee, C. K. Dunn, N. X. Fang, M. L. Dunn, *Sci. Rep.* **2016**, *6*, 31110.
- [111] V. Kumar, Y. K. Bhardwaj, S. Sabharwal, *Prog. Org. Coatings* **2006**, *55*, 316.

- [112] G. Fei, C. Parra-Cabrera, Y. Li, D. E. Kravchenko, R. Dochy, L. Van Looy, R. Ameloot, *Cell Reports Phys. Sci.* **2023**, *4*, 101504.
- [113] F. Liu, X. Jiang, Q. Zhang, M. Zhu, *Compos. Sci. Technol.* **2014**, *101*, 86.
- [114] X. Zhao, Y. Zhao, M. D. Li, Z. Li, H. Peng, T. Xie, X. Xie, *Nat. Commun.* **2021**, *12*, 2873.
- [115] A. Torres-Knoop, I. Kryven, V. Schamboeck, P. D. Iedema, *Soft Matter* **2018**, *14*, 3404.
- [116] D. Ahn, L. M. Stevens, K. Zhou, Z. A. Page, *ACS Cent. Sci.* **2020**, *6*, 1555.
- [117] Y. Bao, N. Paunović, J. Leroux, *Adv. Funct. Mater.* **2022**, *32*, 2109864.
- [118] M. Sandmeier, N. Paunović, R. Conti, L. Hofmann, J. Wang, Z. Luo, K. Masania, N. Wu, N. Kleger, F. B. Coulter, A. R. Studart, H. Grützmacher, J. C. Leroux, Y. Bao, *Macromolecules* **2021**, *54*, 7830.
- [119] M. Zarek, M. Layani, I. Cooperstein, E. Sachyani, D. Cohn, S. Magdassi, *Adv. Mater.* **2016**, *28*, 4449.
- [120] M. Zarek, N. Mansour, S. Shapira, D. Cohn, *Macromol. Rapid Commun.* **2017**, *38*, 1600628.
- [121] A. Oesterreicher, J. Wiener, M. Roth, A. Moser, R. Gmeiner, M. Edler, G. Pinter, T. Griesser, *Polym. Chem.* **2016**, *7*, 5169.
- [122] S. Chen, W. D. Cook, F. Chen, *Polym. Int.* **2007**, *56*, 1423.
- [123] R. Nixon, J. Cahill, R. Jolanki, in *Kanerva's Occup. Dermatology*, Springer, Berlin, Heidelberg **2012**, pp. 559–581.
- [124] J. D. Cho, E. O. Kim, H. K. Kim, J. W. Hong, *Polym. Test.* **2002**, *21*, 781.
- [125] A. Al Mousawi, F. Dumur, P. Garra, J. Toufaily, T. Hamieh, F. Goubard, T. T. Bui, B. Graff, D. Gigmes, J. Pierre Fouassier, J. Lalevée, *J. Polym. Sci. Part A Polym. Chem.* **2017**, *55*, 1189.
- [126] J. Zhang, F. Dumur, P. Xiao, B. Graff, D. Gigmes, J. P. Fouassier, J. Lalevée, *J. Polym. Sci. Part A Polym. Chem.* **2016**, *54*, 1189.
- [127] J. Chen, M. D. Soucek, W. J. Simonsick, R. W. Celikay, *Polymer (Guildf)* **2002**, *43*, 5379.
- [128] B. U. Ahn, S. K. Lee, S. K. Lee, J. H. Park, B. K. Kim, *Prog. Org. Coatings* **2008**, *62*, 258.
- [129] T. Y. Huang, H. W. Huang, D. D. Jin, Q. Y. Chen, J. Y. Huang, L. Zhang, H. L. Duan, *Sci. Adv.* **2020**, *6*, eaav8219.
- [130] Z. Xiong, M. L. Zheng, X. Z. Dong, W. Q. Chen, F. Jin, Z. S. Zhao, X. M. Duan, *Soft Matter* **2011**, *7*, 10353.
- [131] M. R. Lee, I. Y. Phang, Y. Cui, Y. H. Lee, X. Y. Ling, *Small* **2015**, *11*, 740.
- [132] Y. Y. C. Choong, S. Maleksaeedi, H. Eng, P. C. Su, J. Wei, *Virtual Phys. Prototyp.* **2017**, *12*, 77.
- [133] S. H. Song, K. Kim, S. E. Choi, S. Han, H. S. Lee, S. Kwon, W. Park, *Opt. Lett.* **2014**, *39*, 5162.
- [134] H. K. Dave, R. T. Karumuri, A. R. Prajapati, S. R. Rajpurohit, *Rapid Prototyp. J.* **2022**, *28*, 1530.
- [135] A. Bertsch, J. Y. Jézéquel, J. C. André, *J. Photochem. Photobiol. A Chem.* **1997**, *107*, 275.
- [136] W. Cho, E. M. Sachs, N. M. Patrikalakis, D. E. Troxel, *Comput. Des.* **2003**, *35*, 851.
- [137] Y. Pang, Y. Shu, M. Shavezipur, X. Wang, M. A. Mohammad, Y. Yang, H. Zhao, N. Deng, R. Maboudian, T. L. Ren, *Sci. Rep.* **2016**, *6*, 28552.
- [138] J. Atencia, S. Barnes, J. Douglas, M. Meacham, L. E. Locascio, *Lab Chip* **2007**, *7*, 1567.
- [139] I. B. Park, Y. M. Ha, S. H. Lee, *Int. J. Adv. Manuf. Technol.* **2011**, *52*, 545.
- [140] S. Gooran, *J. Imaging Sci. Technol.* **2006**, *50*, 157.
- [141] G. Fei, C. Parra-Cabrera, B. Xia, K. Zhong, K. Clays, R. Ameloot, *Cell Reports Phys. Sci.* **2023**, *4*, 101525.
- [142] L. Huang, R. Jiang, J. Wu, J. Song, H. Bai, B. Li, Q. Zhao, T. Xie, *Adv. Mater.* **2017**, *29*, 1605390.
- [143] Z. Fang, H. Song, Y. Zhang, B. Jin, J. Wu, Q. Zhao, T. Xie, *Matter* **2020**, *2*, 1187.
- [144] Y. Zhang, Q. Zhang, X. Ouyang, D. Y. Lei, A. P. Zhang, H. Y. Tam, *ACS Nano* **2018**, *12*, 9913.
- [145] F. Petko, A. Świeży, J. Ortyl, *Polym. Chem.* **2021**, *12*, 4593.
- [146] M. G. Hennessy, A. Vitale, O. K. Matar, J. T. Cabral, *Soft Matter* **2017**, *13*, 9199.
- [147] Y. A. Chekanov, J. A. Pojman, *J. Appl. Polym. Sci.* **2000**, *78*, 2398.
- [148] I. D. Robertson, M. Yourdkhani, P. J. Centellas, J. E. Aw, D. G. Ivanoff, E. Goli, E. M. Lloyd, L. M. Dean, N. R. Sottos, P. H. Geubelle, J. S. Moore, S. R. White, *Nature* **2018**, *557*, 223.
- [149] Y. Zhang, L. Huang, H. Song, C. Ni, J. Wu, Q. Zhao, T. Xie, *ACS Appl. Mater. Interfaces* **2019**, *11*, 32408.
- [150] M. Fang, T. Liu, Y. Xu, B. Jin, N. Zheng, Y. Zhang, Q. Zhao, Z. Jia, T. Xie, *Adv. Mater.* **2021**, *33*, 2105597.
- [151] J. A. Crowe-Willoughby, K. L. Weiger, A. E. Özçam, *J. Genzer* **2010**, *51*, 763.
- [152] J. Kim, J. A. Hanna, M. Byun, C. D. Santangelo, R. C. Hayward, *Science* **2012**, *335*, 1201.
- [153] C. Chen, D. Hirdes, A. Folch, *Proc. Natl. Acad. Sci.* **2003**, *100*, 1499.
- [154] Y. Jung, H. Lee, T. J. Park, S. Kim, S. Kwon, *Sci. Rep.* **2015**, *5*, 15629.
- [155] C. M. Rackson, K. M. Champley, J. T. Toombs, E. J. Fong, V. Bansal, H. K. Taylor, M. Shusteff, R. R. McLeod, *Addit. Manuf.* **2021**, *48*, 102367.
- [156] B. Deore, K. L. Sampson, T. Lacelle, N. Kredentser, J. Lefebvre, L. S. Young, J. Hyland, R. E. Amaya, J. Tanha, P. R. L. Malenfant, H. W. de Haan, C. Paquet, *Nat. Commun.* **2021**, *12*, 55.
- [157] V. Hahn, P. Kiefer, T. Frenzel, J. Qu, E. Blasco, C. Barner-Kowollik, M. Wegener, *Adv. Funct. Mater.* **2020**, *30*, 1907795.
- [158] Y. Liao, W. Li, Z. Zhan, H. Duan, P. Liu, Y. Chen, Z. Wang, *ACS Omega* **2021**, *6*, 18281.
- [159] P. F. Jacobs, *Rapid Prototyping & Manufacturing: Fundamentals of Stereolithography*, Society Of Manufacturing Engineers, Dearborn, MI, USA **1992**.
- [160] H. Gong, B. P. Bickham, A. T. Woolley, G. P. Nordin, *Lab Chip* **2017**, *17*, 2899.
- [161] R. He, D. Yunus, C. Uhl, W. Shi, S. Sohrabi, Y. Liu, *Microfluid. Nanofluidics* **2017**, *21*, 13.
- [162] A. Rammohan, P. K. Dwivedi, R. Martinez-Duarte, H. Katepalli, M. J. Madou, A. Sharma, *Sens. Actuat. B Chem* **2011**, *153*, 125.
- [163] A. Liu, F. He, K. Wang, T. Zhou, Y. Lu, X. Xia, *Lab Chip* **2005**, *5*, 974.
- [164] M. J. Männel, L. Selzer, R. Bernhardt, J. Thiele, *Adv. Mater. Technol.* **2019**, *4*, 1800408.
- [165] C. Yuan, K. Kowsari, S. Panjwani, Z. Chen, D. Wang, B. Zhang, C. J. X. Ng, P. V. Y. Alvarado, Q. Ge, *ACS Appl. Mater. Interfaces* **2019**, *11*, 40662.
- [166] A. Grushina, *Adv. Opt. Technol.* **2019**, *8*, 163.
- [167] P. Preechaburana, D. Filippini, *Lab Chip* **2011**, *11*, 288.
- [168] C. Williams, G. S. D. Gordon, T. D. Wilkinson, S. E. Bohndiek, *ACS Photonics* **2019**, *6*, 3132.
- [169] X. Li, Z. J. Tan, N. X. Fang, *Optica* **2020**, *7*, 1154.
- [170] H. Zheng, Y. Zhou, C. F. Ugwu, A. Du, I. I. Kravchenko, J. G. Valentine, *ACS Photonics* **2021**, *8*, 1824.
- [171] X. Ma, X. Qu, W. Zhu, Y. S. Li, S. Yuan, H. Zhang, J. Liu, P. Wang, C. S. E. Lai, F. Zanella, G. S. Feng, F. Sheikh, S. Chien, S. Chen, *Proc. Natl. Acad. Sci.* **2016**, *113*, 2206.
- [172] A. M. Kloxin, J. A. Benton, K. S. Anseth, *Biomaterials* **2010**, *31*, 1.
- [173] S. C. P. Norris, P. Tseng, A. M. Kasko, *ACS Biomater. Sci. Eng.* **2016**, *2*, 1309.
- [174] A. M. Kloxin, M. W. Tibbitt, A. M. Kasko, J. A. Fairbairn, K. S. Anseth, *Adv. Mater.* **2010**, *22*, 61.
- [175] K. Kumar, H. Duan, R. S. Hegde, S. C. W. Koh, J. N. Wei, J. K. W. Yang, *Nat. Nanotechnol.* **2012**, *7*, 557.

- [176] J. Wu, Z. Zhao, X. Kuang, C. M. Hamel, D. Fang, H. J. Qi, *Multifunct. Mater.* **2018**, *1*, 015002.
- [177] Q. Zhang, X. Kuang, S. Weng, L. Yue, D. J. Roach, D. Fang, H. J. Qi, *Adv. Funct. Mater.* **2021**, *31*, 2010872.
- [178] S. Miao, N. Castro, M. Nowicki, L. Xia, H. Cui, X. Zhou, W. Zhu, S. Lee, K. Sarkar, G. Vozzi, Y. Tabata, J. Fisher, L. G. Zhang, *Mater. Today* **2017**, *20*, 577.
- [179] M. Hippler, E. Blasco, J. Qu, M. Tanaka, C. Barner-Kowollik, M. Wegener, M. Bastmeyer, *Nat. Commun.* **2019**, *10*, 232.
- [180] M. Champeau, D. A. Heinze, T. N. Viana, E. R. de Souza, A. C. Chinellato, S. Titotto, *Adv. Funct. Mater.* **2020**, *30*, 1910606.
- [181] Y. Hu, Z. Wang, D. Jin, C. Zhang, R. Sun, Z. Li, K. Hu, J. Ni, Z. Cai, D. Pan, X. Wang, W. Zhu, J. Li, D. Wu, L. Zhang, J. Chu, *Adv. Funct. Mater.* **2020**, *30*, 1907377.
- [182] Y. Dong, S. Wang, Y. Ke, L. Ding, X. Zeng, S. Magdassi, Y. Long, *Adv. Mater. Technol.* **2020**, *5*, 2000034.
- [183] Z. Zhao, H. J. Qi, D. Fang, *Soft Matter* **2019**, *15*, 1005.
- [184] H. Ping, W. Wagermaier, N. Horbelt, E. Scoppola, C. Li, P. Werner, Z. Fu, P. Fratzl, *Science* **2022**, *376*, 188.
- [185] D. Mondal, Z. Haghpanah, C. J. Huxman, S. Tanter, D. Sun, M. Gorbet, T. L. Willett, *Mater. Sci. Eng. C* **2021**, *130*, 112456.
- [186] Z. Zhao, X. Kuang, C. Yuan, H. J. Qi, D. Fang, *ACS Appl. Mater. Interfaces* **2018**, *10*, 19932.
- [187] R. Hensleigh, H. Cui, Z. Xu, J. Massman, D. Yao, J. Berrigan, X. Zheng, *Nat. Electron.* **2020**, *3*, 216.
- [188] H. Cui, D. Yao, R. Hensleigh, H. Lu, A. Calderon, Z. Xu, S. Davaria, Z. Wang, P. Mercier, P. Tarazaga, X. (Rayne) Zheng, *Science (80-)*. **2022**, *376*, 1287.
- [189] B. Wagner, H. J. Quenzer, W. Henke, W. Hoppe, W. Pilz, *Sens. Actuat. A Phys.* **1995**, *46*, 89.
- [190] Z. Cui, J. Du, Y. Guo, in *Micromach. Technol. Micro-Optics Nano-Optics*, **2003**, (Ed.: E. G. Johnson), p. 111.
- [191] X. Mu, T. Bertron, C. Dunn, H. Qiao, J. Wu, Z. Zhao, C. Saldana, H. J. Qi, *Mater. Horiz.* **2017**, *4*, 442.
- [192] Y. Kim, H. Yuk, R. Zhao, S. A. Chester, X. Zhao, *Nature* **2018**, *558*, 274.
- [193] N. Annabi, J. W. Nichol, X. Zhong, C. Ji, S. Koshy, A. Khademhosseini, F. Dehghani, *Tissue Eng. Part B Rev.* **2010**, *16*, 371.



Guanghai Fei is a postdoctoral researcher under the supervision of Prof. Rob Ameloot at cMACS, Department of Microbial and Molecular Systems, KU Leuven, Belgium. He received his Ph.D. in bio-science engineering from KU Leuven in 2022. His research interest lies in stereolithography 3D printing of composites, graded materials, and porous materials.



Rob Ameloot is a professor at cMACS, Department of Microbial and Molecular Systems, KU Leuven, Belgium. He obtained his Ph.D. at KU Leuven and was a Fulbright postdoctoral fellow at the University of California, Berkeley (US). His research interest focuses on enabling applications based on porous materials through a fundamental understanding of their formation processes and properties.